NATIONAL CENTER FOR EARTHQUAKE
ENGINEERING RESEARCH
State University of New York at Buffalo

MULTI-HAZARD RISK ANALYSIS: CASE OF A SIMPLE OFFSHORE STRUCTURE

by

B.K. Bhartia and E.H. Vanmarcke
Department of Civil Engineering and Operations Research
Princeton University
Princeton, New Jersey 08544

Technical Report NCEER-88-0023

July 21, 1988

This research was conducted at Princeton University and was partially supported by the National Science Foundation under Grant No. ECE 86-07591.

NOTICE

This report was prepared by Princeton University as a result of research sponsored by the National Center for Earthquake Engineering Research (NCEER). Neither NCEER, associates of NCEER, its sponsors, Princeton University or any person acting on their behalf:

a. makes any warranty, express or implied, with respect to the use of any information, apparatus, method, or process disclosed in this report or that such use may not infringe upon privately owned rights; or

b. assumes any liabilities of whatsoever kind with respect to the use of, or the damage resulting from the use of, any information, apparatus, method or process disclosed in this report.

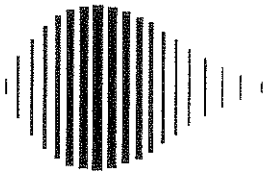

MULTI-HAZARD RISK ANALYSIS: CASE OF A SIMPLE OFFSHORE STRUCTURE

by

B.K. Bhartia[1] and E.H. Vanmarcke[2]

July 21, 1988

Technical Report NCEER-88-0023

NCEER Contract Number NCEER-87-3002

NSF Master Contract Number ECE 86-07591

1 Graduate Student, Dept. of Civil Engineering, Princeton University
2 Professor, Dept. of Civil Engineering, Princeton University

NATIONAL CENTER FOR EARTHQUAKE ENGINEERING RESEARCH
State University of New York at Buffalo
Red Jacket Quadrangle, Buffalo, NY 14261

PREFACE

The National Center for Earthquake Engineering Research (NCEER) is devoted to the expansion and dissemination of knowledge about earthquakes, the improvement of earthquake-resistant design, and the implementation of seismic hazard mitigation procedures to minimize loss of lives and property. The emphasis is on structures and lifelines that are found in zones of moderate to high seismicity throughout the United States.

NCEER's research is being carried out in an integrated and coordinated manner following a structured program. The current research program comprises four main areas:

- Existing and New Structures
- Secondary and Protective Systems
- Lifeline Systems
- Disaster Research and Planning

This technical report pertains to Program 1, Existing and New Structures, and more specifically to Reliability Analysis and Risk Assessment.

The long term goal of research in Existing and New Structures is to develop seismic hazard mitigation procedures through rational probabilistic risk assessment for damage or collapse of structures, mainly existing buildings, in regions of moderate to high seismicity. This work relies on improved definitions of seismicity and site response, experimental and analytical evaluations of systems response, and more accurate assessment of risk factors. This technology will be incorporated in expert systems tools and improved code formats for existing and new structures. Methods of retrofit will also be developed. When this work is completed, it should be possible to characterize and quantify societal impact of seismic risk in various geographical regions and large municipalities. Toward this goal, the program has been divided into five components, as shown in the figure below:

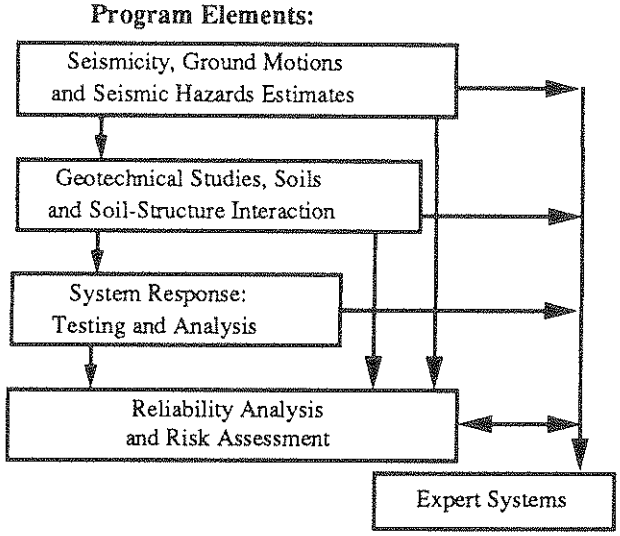

Tasks:

Earthquake Hazards Estimates,
Ground Motion Estimates,
New Ground Motion Instrumentation,
Earthquake & Ground Motion Data Base.

Site Response Estimates,
Large Ground Deformation Estimates,
Soil-Structure Interaction.

Typical Structures and Critical Structural Components:
Testing and Analysis;
Modern Analytical Tools.

Vulnerability Analysis,
Reliability Analysis,
Risk Assessment,
Code Upgrading.

Architectural and Structural Design,
Evaluation of Existing Buildings.

Reliability Analysis and Risk Assessment research constitutes one of the important areas of Existing and New Structures. Current research addresses, among others, the following issues:

1. Code issues - Development of a probabilistic procedure to determine load and resistance factors. Load Resistance Factor Design (LRFD) includes the investigation of wind vs. seismic issues, and of estimating design seismic loads for areas of moderate to high seismicity.
2. Response modification factors - Evaluation of RMFs for buildings and bridges which combine the effect of shear and bending.
3. Seismic damage - Development of damage estimation procedures which include a global and local damage index, and damage control by design; and development of computer codes for identification of the degree of building damage and automated damage-based design procedures.
4. Seismic reliability analysis of building structures - Development of procedures to evaluate the seismic safety of buildings which includes limit states corresponding to serviceability and collapse.
5. Retrofit procedures and restoration strategies.
6. Risk assessment and societal impact.

Research projects concerned with Reliability Analysis and Risk Assessment are carried out to provide practical tools for engineers to assess seismic risk to structures for the ultimate purpose of mitigating societal impact.

This study focuses on developing and illustrating a methodology for multi-mode, multi-hazard risk assessment. In this report, both short-term and long-term multi-hazard risk analyses of an off-shore platform are made. The authors also determine the influence of ambient load on the earthquake safety and the effect of parameter uncertainty on failure probabilities.

Abstract

This report develops and illustrates methodology for multi-mode, multi-hazard risk assessment. The case study involves an offshore structure subjected to earthquake shaking and storm-generated wind, wave, and current loads. Two classes of risks are calculated: (1) conditional failure probabilities under short-term loads; and (2) long-term or overall risks, which depend on occurrence patterns of loads of different intensities. These risks are calculated for several combinations of earthquake and storm loads including the ambient load based on two limit states, both of the first passage type, respectively defined in terms of allowable displacement and acceleration at the deck level of the structure. Drift or dynamic displacement often controls the design of tall structures, while acceleration limit state is useful in assessing the risk to secondary systems or acceleration-sensitive instruments mounted on the deck. This report accounts explicitly for two distinct sources of uncertainty in the risk assessment: one is inherent, essentially irreducible uncertainty, e.g., due to random phasing of sinusoids in earthquake ground motion, and the other, statistical uncertainty of load and structural parameters. In the case study, the structure is modeled as a single-degree linear system with the response analysis performed in the frequency domain using linear random vibration theory.

This report shows that the relative importance of different loads depends on the limit states and on the load and structural characteristics. For a flexible offshore structure, the storm load dominates in the case of a displacement limit state, but is unimportant compared to the earthquake load in relation to an acceleration limit state. Parameter uncertainty is shown to always increase the long-term risk; in the case study, the increase is more pronounced for the displacement limit state than for the acceleration limit state. Also, it is shown that the ambient load increases the risk due to earthquake loads alone, especially at the lower resistance levels.

ACKNOWLEDGEMENT

This research was supported by the National Science Foundation through the National Center for Earthquake Engineering Research under Agreement NCEER-87-3002 on "Earthquake Engineering: Multi-Hazard Risk Assessment and Management." Any opinions, findings and conclusions or recommendations are those of the authors and do not necessarily reflect the views of the National Science Foundation.

TABLE OF CONTENTS

TABLE OF CONTENTS (Cont'd)

LIST OF ILLUSTRATIONS

LIST OF ILLUSTRATIONS (Cont'd)

LIST OF ILLUSTRATIONS (Cont'd)

LIST OF TABLES

1. Introduction

Multi-hazard risk analysis is concerned with the performance of structures subjected to multiple random loads, some of which may occur simultaneously. To focus and illustrate the presentation of the methodology, this report examines a simple model of an offshore structure subjected to earthquake shaking and sea-storm-generated wind, wave, and current loads. We compute the integrated risk in the presence of multiple loads and determine the relative importance of different loads in function of both the structural and load characteristics.

A detailed risk analysis is presented of an offshore oil-platform exposed to four different combinations of earthquake and sea-storm loads. The load combinations are: (1) earthquake load alone, (2) earthquake load plus ambient load, (3) sea-storm load alone, and (4) earthquake load plus sea-storm load. The ambient load of the second load combination arises due to the ever-present wind over the sea, and is included herein to study its impact on the earthquake safety.

In general, "failure" is said to occur when the structure or one of its components reaches a "limit state," i.e., a condition of undesirable behavior or performance. This report calculates the probabilities of structural failure based on two limit states, defined, respectively, in terms of relative displacement and (pseudo) acceleration at the deck level of the structure. The acceleration limit state is relevent in assessing the safety of secondary systems or acceleration-sensitive instruments mounted on the deck. Two classes of failure probabilities are calculated: (1) conditional failure probabilities under short-term loads; and (2) long-term or overall failure probabilities, which depend on occurrence patterns of different load intensities.

We account explicitly for two distinct sources of uncertainty in evaluating the probabilities of a structural failure. One is inherent, irreducible, uncertainty, e.g., due to random phasing of sinusoids in earthquake ground motion; and the other is statistical uncertainty of the load and structural parameters. The latter uncertainty reflects the fact that limited data are available for the load and structural characteristics to which probability distributions are assigned instead of deterministic point values. This report seeks to evaluate the effect of this parameter uncertainty on response statistics and failure probabilities.

The response analysis herein is performed in the frequency domain using linear random vibration theory, i.e., the equations of motion are linearized based on equivalent linearization

techniques. Also, the response to both earthquake and sea-storm loads is assumed to be quasi-stationary during load events of specified durations.

2. Dynamic Model

For a case study, this report considers a three-legged offshore oil-platform, 80 meters deep, shown in Fig. 2.1. The structure is modeled as a 1-DOF system with only the horizontal motion. The rotational motion or the vertical drop of the deck are being neglected. The deck structure for the purpose of the wind load calculation is modeled as an equivalent rectangular wall normal to the mean wind direction, with height h and width b. The three legs, tubular in form, are assumed to have full end fixity. Fig. 2.1b shows a dynamic model of the structure with the dominant mode shape, $\psi(z)$, shown by the dashed line, given as

$$\psi(z) = 1 - \cos\left(\frac{\pi z}{2l}\right), \tag{2.1}$$

where z is the vertical axis with origin at the sea surface, and l the length of the legs. Table 2.1 lists the structure's dynamic characteristics and other important dimensions. The values for modal mass M, stiffness K, and natural frequency ω_n are calculated based on the mode shape $\psi(z)$ and the modal damping ratio ζ is assumed to be 4.0 %.

To calculate the modal mass, we lump a fraction f_m of the virtual mass of the three legs with the deck mass:

$$M = m_d + 3[\bar{m}d + \bar{m}_0(l-d)]f_m, \tag{2.2}$$

where m_d is the deck-mass, $\bar{m}_0$ and $\bar{m}$ the actual and virtual mass per unit length of a single leg, respectively, d the water depth, and $(l-d)$ the length of a leg between the still water level and the bottom of the deck. Factor f_m based on the modal analysis [16] is found to be 0.375. The modal stiffness is calculated as

$$K = 36EI/l^3, \tag{2.3}$$

which is the magnitude of the horizontal force at the deck level that produces a unit deflection at that point. E is the Young's modulus of elasticity and I the rotational moment of inertia. Thus, the natural frequency of the structure can be written as

$$\omega_n = \sqrt{K/M}. \tag{2.4}$$

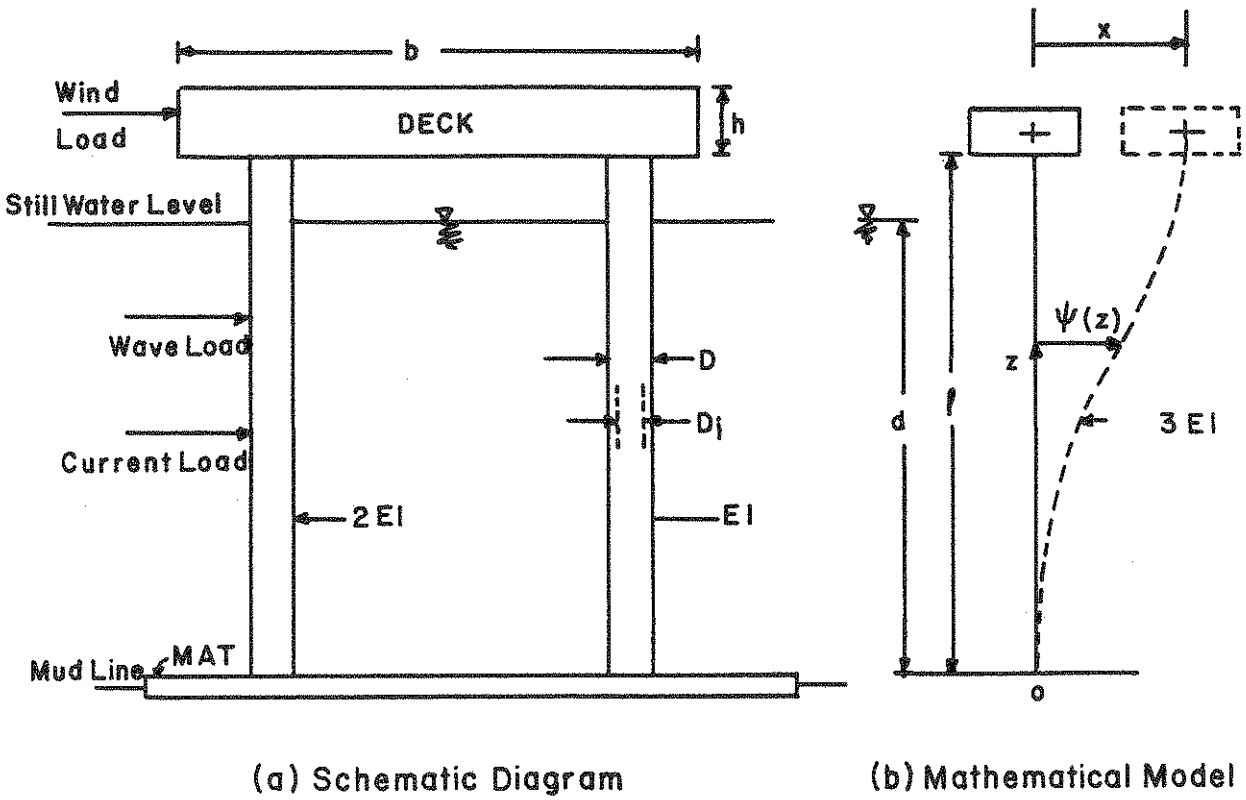

FIGURE 2-1 Model of a Jack-Up Type Oil Platform

Table 2.I Dynamic Characteristics and Some Dimensions of the Platform

modal mass (kg)	M	5.44×10^6
modal stiffness (N/m)	K	2.67×10^7
modal natural freq. (rad/sec)	ω_n	2.21
length of legs (m)	l	80.0
submerged depth (m)	d	72.0
deck-width (m)	b	50.0
deck-height (m)	h	5.0
leg-dia (outer) (m)	D	3.7

3. Modeling of Environmental Loads

Short-term and long-term models for earthquake, wind, wave, and current loads are presented below. The short-term characterization is concerned with the details of the load time history during each load event, while the long-term model describes the recurrence pattern of potentially damaging load events.

3.1 Earthquake Load

Earthquakes at a site occur as a sequence of events which are generally nonstationary with respect to frequency content and intensity. For the purpose of stochastic analysis, however, motions during each load event are modeled as limited duration segments of stationary random processes.

3.1.1 Seismic Hazard

The seismic hazard at a site is described through a plot of annual exceedence probability versus the peak ground acceleration A_p. Over the range of a-values significant to structural risk analysis, it is represented as

$$P[A_p > a] = 1 - \exp\left[-\left(\frac{\mu}{a}\right)^{\kappa}\right], \tag{3.1}$$

which has the form of a type-II extreme value distribution. κ and μ are the size and shape parameters of the distribution, chosen here to be 2.7 and 0.18, respectively [6].

3.1.2 Spectral Density Function

The one-sided spectral density function (SDF) of ground acceleration on bedrock is modeled by [13]:

$$G_A(\omega) = G_0[1 + (\omega_0/\omega)^2]^{-2} \exp(-\omega/\omega_r), \tag{3.2}$$

where G_0 = the intensity parameter, ω_0 = the corner frequency, $\omega_r = \pi(r_1/r)$, r = the epicentral distance in km, $r_1 = \gamma^{-1}$ = the characteristic decay (e^{-1}) distance for the 1-sec wave amplitude in km/sec.

Assuming that ω_0 is small compared with ω_r, which is the case most of the time, an integration of Eq. 3.2 with respect to ω yields the following expression for the variance of ground acceleration:

$$\sigma_A^2 = \int G_A(\omega)\, d\omega \simeq G_0\, \omega_r. \tag{3.3}$$

Also, the square root of the variance of ground acceleration can be expressed as the peak ground acceleration A_p divided by a peak factor, assumed here to be 2.75:

$$\sigma_A \simeq A_p/2.75. \tag{3.4}$$

Thus, from Eqs. 3.3 and 3.4,

$$G_0 = \frac{(A_p/2.75)^2}{\omega_r}, \tag{3.5}$$

which relates the spectral intensity G_0 to the peak ground acceleration A_p. The long-term distribution of A_p is expressed in terms of the curve of site seismic hazard.

The strong motion durations for earthquake load events are uncertain. Their variability is important especially in the context of nonlinear response. This report, however, treats only the linear response, and, as a first approximation, assumes a constant duration for each load event, set equal to 20 sec.

3.2 Wind Load

Structures exposed to gusty wind experience a fluctuating wind load. Assuming a quasi-stationary wind drag coefficient, C_d, the wind load, $F(t)$, may be expressed as

$$F(t) = \frac{1}{2}\rho_a a C_d V^2(t), \tag{3.5}$$

where ρ_a is the density of air, a the exposed area of the structure normal to the mean wind, and $V(t)$ the fluctuating wind velocity. Wind load phenomena other than turbulence such as vortex-shedding, galloping, and flutter are not considered. The wind velocity $V(t)$ is resolved into a time-independent mean value $\bar{V}$ and a stationary fluctuating part $v(t)$:

$$V(t) = \bar{V} + v(t). \tag{3.6}$$

When the fluctuations are small compared with the mean wind, Eq. 3.5 for the wind load can be linearized:

$$F(t) \simeq \frac{1}{2}\rho_a a C_d \left(\bar{V}^2 + 2|\bar{V}|v(t)\right), \tag{3.7}$$

where the first term gives static load, and the second dynamic load in the direction of mean wind.

3.2.1 Statistics of Wind Velocity

The annual maxima of mean wind velocity in the United States is often assumed to follow the type-II extreme value distribution:

$$P[\bar{V} < v] = \exp\left[-\left(\frac{u}{v}\right)^k\right], \tag{3.8}$$

in which u and k are the size and shape parameters of the distribution. For illustrative purposes, we use parameters determined from a set of wind data observed at Logan airport, Boston, Massachusetts [1]. Parameter u is found to be 91.2 km per hour, and k, 8.8. The annual maximum mean wind corresponding to a $\bar{T}$ year return period can be obtained from the following relation:

$$P[\bar{V} < v] = 1 - \frac{1}{\bar{T}(v)}. \tag{3.9}$$

Though the mean wind in a natural wind increases with the height, since the wind load for offshore structures constitutes a secondary load, the mean wind throughout the structure's exposed area is assumed to be the same, equal to the mean wind at a height of 10 m from the sea surface, $\bar{V}_{10}$.

3.2.2 Spectral Density Function of Fluctuating Wind Component

The SDF of fluctuating wind component is modeled by the Davenport spectrum [4]:

$$G_v(\omega) = \frac{4\,k_r \bar{V}_{10}^2\, X^2}{\omega(1+X^2)^{4/3}}, \tag{3.10}$$

where

$$X = \frac{\omega L}{2\pi \bar{V}_{10}}.$$

X is a dimensionless variable, ω the circular frequency, L the length parameter, taken as 1200 m, and k_r the terrain roughness parameter. The suggested values of k_r for smooth, medium and rough surfaces are 0.005, 0.015, and 0.05, respectively.

The strong motion duration for each storm event is assumed to be 20 minutes.

3.3 Wave Load

The wave load on structures is usually described in terms of sea states. A sea state is an approximately stationary condition described by parameters with long-term fluctuations. These parameters include the significant wave height, H_s, and the mean wave period, T_s.

3.3.1 Wave Height Spectrum

The SDF of wave height in a fully developed sea is modeled in terms of mean wind velocity, $\bar{V}_{10}$, by the Pierson-Moskowitz spectrum [11]:

$$G_H(\omega) = \frac{\alpha g^5}{\omega^5} \exp\left(-\frac{\beta g^4}{\bar{V}_{10}^4 \omega^4}\right), \tag{3.11}$$

where g is the acceleration due to gravity, and α and β the spectral parameters. Common values $\alpha = 0.0081$ and $\beta = 0.74$ are adopted.

The significant wave height, H_s, and the mean wave period, T_s, are related to the first two moments of the wave spectrum, and hence uniquely determined by the mean wind $\bar{V}_{10}$. The mean wind thus provides a useful common base to determine the wind, wave, and current loads.

3.3.2 Gravity Waves

The kinematics of water particle below the sea surface can be related to the wave height through a wave theory. Several theories with various degrees of refinements are available, but stochastic description of wave forces are generally limited to the linear theory of gravity waves. This theory gives the particle velocity and acceleration, and the dispersion relationship as follows:

$$u(z,t) = \frac{\omega H}{2} \frac{\cosh kz}{\sinh kd} \cos \omega t, \tag{3.12}$$

$$\dot{u}(z,t) = \frac{\omega^2 H}{2} \frac{\cosh kz}{\sinh kd} \sin \omega t, \tag{3.13}$$

$$\omega^2 = kg \tanh kd, \tag{3.14}$$

where u is the particle velocity, $\dot{u}$ the particle acceleration, k the wave number, and d the water depth.

3.3.3 Wave Forces and Morison's Formula

For waves with large wavelengths, the wave load on structures is made up of two components: a drag force, proportional to the square of the normal component of incident particle velocity; and an inertia force, associated with the normal component of particle acceleration. For an oscillating cylinder, the wave force per unit lenght, $F(t)$, is given as [10]:

$$F(t) = \frac{1}{2} C_d \rho_w a \left| u(t) - \dot{x}(t) \right| \left(u(t) - \dot{x}(t) \right) + C_m \rho_w b \dot{u}(t) - (C_m - 1) \rho_w b \ddot{x}(t), \tag{3.15}$$

where C_d is the drag coefficient, C_m the inertia coefficient, ρ_w the density of water, b the volume of member, a the projected area of member perpendicular to the motion of fluid, and $x(t)$ the displacement of the structure. Denoting the relative velocity between water particles and structure by $u_r(t)$, where

$$u_r(t) = u(t) - \dot{x}(t), \tag{3.16}$$

the drag force in Eq. 3.15 can be written as

$$F_D(t) = \frac{1}{2} C_d \rho_w a \left| u_r(t) \right| u_r(t). \tag{3.17}$$

The nonlinear drag force for a stochastic analysis is linearized by means of equivalent linearization techniques [1,5]: the nonlinear term $|u_r(t)|u_r(t)$ is replaced with a linear term $d_r u(t)$ such that the linearized drag factor, d_r, minimizes the mean squared error. Assuming that $u_r(t)$ constitutes a Gaussian process, the equivalent linearization yields

$$d_r = \sqrt{8/\pi}\, \sigma_{u_r}. \tag{3.18}$$

The wave forces, Eq. 3.15, can now be expressed in the following linearized form:

$$F(t) = \frac{1}{2} C_d \rho_w a d_r \left(u(t) - \dot{x}(t) \right) + C_m \rho_w b \dot{u}(t) - (C_m - 1) \rho_w b \ddot{x}(t). \tag{3.19}$$

As evident in Eq. 3.19, the wave force depends on the water particle motion as well as on the structure's motion. But, since the structure's motion is expected to be small compared with the water particle motion, the dependence of wave force on the structure's motion is ignored. It should be noted, however, that this dependence can be easily incorporated by including the virtual inertia and hydrodynamic drag forces in the equations of motion, and obtaining the statistics of relative motion through iteration, which is found to converge quickly [9].

3.4 Current Load

Wind flow over the sea surface generates wind-stressed current in the direction of mean wind, with the current velocity given as

$$u_c(d) = c\,\bar{V}_{10}, \tag{3.20}$$

where $u_c(d)$ is the current velocity at sea surface, and c a proportionality constant, 1–5 %. The current velocity decreases linearly with depth, dropping to zero at the sea bottom. The current load on structures is mostly static and predominantly of the drag type.

4. Parameter Uncertainty

Due to a limited database, there exists statistical uncertainty about the parameters such as those in the spectral density functions of the loads, load-to-force conversions, and mathematical model of the structure. To reflect this uncertainty and to account for its effect on the estimates of response statistics and failure probabilities, these parameters can be assigned probability distributions. The parameters so treated include ω_0 and ω_r in the ground acceleration spectrum, k_r in the fluctuating wind spectrum, α and β in the wave height spectrum, the drag coefficient C_d, the inertia coefficient C_m, the wind-stressed current coefficient c, the structure's natural frequency ω_n, and the structure's damping ratio ζ. The long-term model parameters, which describe the occurrence patterns of earthquake and sea-storm loads, and the load event durations are still treated as deterministic parameters. Their treatment as uncertain parameters, however, would be a simple extension.

A common underlying feature of the parameters mentioned is that they all take only positive values. This report models these parameters as lognormally distributed. The choice of lognormal distribution though is not believed to be critical. The point is that in the expressions for the response statistics we assume lognormality for certain combinations (products or quotients) of random variables. Even if the individual random variables are not lognormal, the product or quotients tends to become lognormal by virtue of the central limit theorem.

The following notations should be noted.

Let X be a lognormal variable, m_X and σ_X the mean and standard deviation of X, and λ_X and ξ_X the mean and standard deviation of logarithm of X. Then, the following relations hold:

$$\xi_X^2 = \ln(1 + \sigma_X^2/m_X^2), \tag{4.1}$$

$$\lambda_X = \ln m_X - \frac{1}{2}\xi_X^2. \tag{4.2}$$

If the coefficient of variation of X $(= \sigma_X/m_X)$ is small, say less than 0.3, we may write

$$\xi_X \simeq \sigma_X/m_X. \tag{4.3}$$

Also note that

$$m_{X^{1/2}} = (m_X)^{1/2} \exp(-\xi_X^2/8). \tag{4.4}$$

Table 4.1 lists the first two statistical moments of the parameters whose uncertainty is accounted for.

The total variability of load or response quantities is made up of the inherent uncertainty (R) and the statistical uncertainty (U); the moments of load or response quantities are subscripted by R or U to indicate the type of uncertainty. Thus, $\sigma_{X,R}$ denotes the standard deviation of X that arises due to the inherent uncertainty, whereas $\sigma_{X,U}$, that due to the statistical uncertainty.

Table 4.I Statistics of Uncertain Parameters

Parameter (X)	m_x	ξ_x
ω_o	$\pi/2$	0.1
ω_r	10π	0.1
κ_r	0.007	0.5
α	0.0081	0.1
β	0.74	0.1
C_d	0.8	0.1
C_m	1.5	0.25
c	0.03	0.5
T_n	2.84 Sec	0.15
ζ	0.04	0.25

5. Response Analysis

The response analysis to dynamic loads is performed in the frequency domain using linear random vibration theory, with forcing functions assumed to constitute segments of stationary Gaussian processes. The response processes are also Gaussian. Based on a stationary response analysis, this section presents the conditional statistics of peak response for load events involving earthquake only, sea-storm only, earthquake plus sea-storm, and, finally, earthquake plus ambient vibration. The response statistics presented are always conditional on the load intensities characterizing each load events.

5.1 Response to Earthquake Load

Let the SDF of ground acceleration at the structure's base be $\hat{G}_A(\omega)$. If there is a soil layer in between the structure's base and bedrock, $\hat{G}_A(\omega)$ can be obtained as

$$\hat{G}_A(\omega) = |H_s(\omega)|^2 G_A(\omega), \tag{5.1}$$

where $G_A(\omega)$ is the SDF of ground acceleration at the bedrock, given by Eq. 3.2, and $H_s(\omega)$ the frequency transfer function of the soil layer. We assume that the structure is founded on firm ground or bedrock, in which case $H_s(\omega) = 1.0$. If the situation varies, $H_s(\omega)$ may be used to reflect the effect of local soil [7,13].

Denoting the structure's relative displacement response as X_e, the response spectrum $G_{X_e}(\omega)$ can be related to the input spectrum $\hat{G}_A(\omega)$ through a frequency-dependent amplification function, $H_e(\omega)$:

$$G_{X_e}(\omega) = |H_e(\omega)|^2 \hat{G}_A(\omega), \tag{5.2}$$

where $H_e(\omega)$ is the relative displacement response of the structure to a sinusoidal accelaration of unit amplitude and frequency ω:

$$H_e(\omega) = [(\omega_n^2 - \omega^2) + i2\zeta\omega\omega_n]^{-1}. \tag{5.3}$$

Also, the variance of relative displacement, $\mathrm{Var}[X_e]$, can be obtained as the area under its SDF:

$$\mathrm{Var}[X_e] = \int_0^\infty G_{X_e}(\omega)\, d\omega. \tag{5.4}$$

The SDF $G_{X_e}(\omega)$, however, contains parameters such as ω_n, ζ, ω_0, ω_r, etc. which possess statistical uncertainty. $\mathrm{Var}[X_e]$ thus is seen as a random variable. The 'mean' of $\mathrm{Var}[X_e]$ corresponds to the 'variance' of X_e attributed to the inherent uncertainty of the ground acceleration. Denoted here as $\sigma^2_{X_e,R}$, the mean of $\mathrm{Var}[X_e]$ is determined by evaluating the integral (5.4) with the mean values substituted for the uncertain parameters. The 'variance' of $\mathrm{Var}[X_e]$ stems from the statistical uncertainty of the load and structural parameters, and is calculated herein as follows: A white-noise approximation for $\mathrm{Var}[X_e]$ can be written as

$$\mathrm{Var}[X_e] \simeq \frac{\pi}{4\zeta\omega_n^3} G_A(\omega_n) \tag{5.5}$$

$$= a_1 \frac{1}{\zeta\omega_n^3} f_1 f_2,$$

where

$$f_1 = \frac{\exp(-\omega_n/\omega_r)}{[1+(\omega_0/\omega_n)^2]},$$

$f_2 = |H_s(\omega_n)|^2$, and $a_1 = \pi G_0/4 =$ deterministic quantity. The right hand side of Eq. 5.5 contains parameters and factors which, though uncertain, take only positive values. Invoking the central limit theorem, $\mathrm{Var}[X_e]$, thus, may be modeled as a lognormal random variable, regardless of the form of the distributions of the underlying parameters. Now assuming independence among the terms on the right side of Eq. 5.5, and following the notation of section four,

$$\xi_e^2 = \mathrm{Var}[\log(\mathrm{Var}[X_e])] \tag{5.6}$$

$$= \xi_\zeta^2 + 9\xi_{\omega_n}^2 + \xi_{f_1}^2 + \xi_{f_2}^2.$$

The moments of factors f_1 and f_2 are obtained through Taylor series expansion.

For a stationary response, the variance of pseudo acceleration is directly related to that of the relative displacement:

$$\mathrm{Var}\left[\ddot{X}_e\right] = \omega_n^4 \mathrm{Var}[X_e]. \tag{5.7}$$

Thus, the statistics of acceleration response can be obtained in a similar fashion as above.

5.1.1 Peak Response

The peak value of mean-zero Gaussian response process X_e can be expressed as

$$X_{pe} = Z(\mathrm{Var}[X_e])^{1/2}, \tag{5.8}$$

where Z is a random peak factor. According to Davenport (1964):

$$m_Z = \sqrt{2 \ln \nu_0^+ t_0} + \frac{0.557}{\sqrt{2 \ln \nu_0^+ t_0}}, \tag{5.9}$$

$$\sigma_Z = \frac{\pi}{6} \frac{1}{\sqrt{2 \ln \nu_0^+ t_0}}, \tag{5.10}$$

in which ν_0^+ is the mean zero up-crossing rate and t_0 the duration of the stationary response process. Here, ν_0^+ is assumed to be equal to the structure's mean natural frequency (in cycles per sec) and t_0 is 20 sec.

The right hand side of Eq. 5.8 may be seen as a product of two random variables, the second of which is random owing to the parameter uncertainty. Making use of the statistics of Z and Var $[X_e]$, the first two moments of X_{pe} can be shown as

$$m_{X_{pe}} = m_Z[\sigma^2_{X_e,R} \exp(-\xi_e^2/4)]^{1/2}. \tag{5.11}$$

$$\sigma^2_{X_{pe},R} = \sigma_Z^2 \sigma^2_{X_e,R}. \tag{5.12}$$

$$\sigma^2_{X_{pe},U} = m_Z^2\{\sigma^2_{X_e,R}[1 - \exp(-\xi_e^2/4)]\}. \tag{5.13}$$

Recall that the subscripts R and U indicate the variability due to the inherent uncertainty and the statistical uncertainty, respectively. Thus, Eq. 5.13 gives the response variance that exists solely due to the parameter uncertainty.

For the purpose of risk analysis, let the conditional peak load-effect be denoted as L_a, where the subscript a indicates the response dependence on the ground motion intensity. Then,

$$m_{L_a} = m_{X_{pe}}. \tag{5.14}$$

$$\sigma^2_{L_a} = \sigma^2_{X_{pe},R} + \sigma^2_{X_{pe},U}. \tag{5.15}$$

Note in Eq. 5.15 that for risk analysis the variances of peak response due to both the inherent randomness and the parameter uncertainty are added together. Furthermore, the conditional peak response is assumed to be lognormally distributed, with the mean and variance given in Eqs. 5.14 and 5.15, respectively. This format is similar to that used in probabilistic risk assessment in the nuclear industry [3].

5.2 Response to Sea-storm Load

A sea-storm induces a wind load having both static and dynamic components, a wave load with only dynamic component, and a current load with only static component. The response to a sea-storm load thus constitutes a random process with non-zero mean.

5.2.1 Static Response

The total static load, denoted as F, is the sum of drag forces due to wind and current:

$$F = F_1 + F_2. \tag{5.16}$$

The static component of wind drag, F_1, is given by Eq. 3.7:

$$F_1 = \frac{1}{2} C_d \rho_a h b \bar{V}_{10}^2, \tag{5.17}$$

where F_1 is conditional on mean wind, $\bar{V}_{10}$, and contains an uncertain parameter, C_d. Knowing the statistics of C_d, the first two moments of F_1 can be found, which for a lognormal C_d are

$$m_1 = \frac{1}{2} m_{C_d} \rho_a h b \bar{V}_{10}^2. \tag{5.18}$$

$$\xi_{1,U} = \xi_{C_d}. \tag{5.19}$$

The drag force due to current, F_2, integrated over the submerged depth of the legs becomes:

$$\begin{aligned} F_2 &= N \int_0^d \frac{1}{2} C_d \rho_w D u_c^2(z)\, dz \\ &= \frac{1}{6} N C_d \rho_w D u_c^2(d), \end{aligned} \tag{5.20}$$

where N is the number of legs, three in this case. On introducing Eq. 3.20, we obtain

$$F_2 = \frac{1}{6} N C_d \rho_w D d c^2 \bar{V}_{10}^2. \tag{5.21}$$

The coefficients C_d and c in Eq. 5.21 are taken to be lognormally distributed; assuming independence and owing to their multiplicative form, the first two moments of F_2 are

$$m_2 = \frac{1}{6} N m_{C_d} \rho_w D d m_c^2 \bar{V}_{10}^2. \tag{5.22}$$

$$\xi_{2,U} = (\xi_{C_d}^2 + 4\xi_c^2)^{1/2}. \tag{5.23}$$

If F_1 and F_2 are assumed independent, the first two moments of F can be written as

$$m_F = m_{F_1} + m_{F_2}. \tag{5.24}$$

$$\begin{aligned} \sigma_{F,U}^2 &= \sigma_{1,U}^2 + \sigma_{2,U}^2 \\ &= m_1^2[\exp(\xi_{1,U}^2) - 1] + m_2^2[\exp(\xi_{2,U}^2) - 1]. \end{aligned} \tag{5.25}$$

The total static displacement, X_s, then becomes:

$$X_s = F/K, \tag{5.26}$$

where K is the modal stiffness. Thus,

$$m_{X_s} = m_F/K. \tag{5.27}$$

$$\sigma_{X_s,U} = \sigma_{F,U}/K. \tag{5.28}$$

5.2.2 Dynamic Response

The total dynamic load, denoted as P, consists of wind drag, wave drag, and wave inertia:

$$P = P_1 + P_2 + P_3. \tag{5.29}$$

Likewise, the response is a sum of the responses due to each of these loads.

5.2.2.1 Wind Drag

Following Eq. 3.7, the dynamic component of wind drag is calculated as

$$P_1 = C_d \rho_a h b \bar{V}_{10} v(t). \tag{5.30}$$

The SDF of the wind drag force, $G_1(\omega)$, can then be related to the SDF of the fluctuating wind component:

$$G_1(\omega) = T_1^2 G_v(\omega), \tag{5.31}$$

where $G_v(\omega)$ is given by Eq. 3.10 and T_1, conditional on the mean wind velocity $\bar{V}_{10}$ is

$$T_1 = C_d \rho_a h b \bar{V}_{10}. \tag{5.32}$$

Denoting the structure's relative displacement as X_1, its SDF, $G_{X_1}(\omega)$, is obtained by

$$G_{X_1}(\omega) = |H(\omega)|^2 G_1(\omega), \tag{5.33}$$

where $H(\omega)$ is the structure's amplification function, i.e., the relative displacement response to a sinusoidal force with unit amplitude and frequency ω:

$$H(\omega) = \{M[(\omega_n^2 - \omega^2) + i2\zeta\omega\omega_n]\}^{-1}, \tag{5.34}$$

where M is the modal mass. The variance of X_1 can be obtained as the area beneath its SDF:

$$\mathrm{Var}\,[X_1] = \int_0^\infty G_{X_1}(\omega)\, d\omega. \tag{5.35}$$

Again, since $G_{X_1}(\omega)$ contains uncertain parameters, $\mathrm{Var}\,[X_1]$ is seen as a random variable. The mean of $\mathrm{Var}\,[X_1]$, denoted as $\sigma^2_{X_1,R}$, is obtained by evaluating the integral (5.35) with the mean values substituted for the uncertain parameters. The variance of $\mathrm{Var}\,[X_1]$ attributed to the statistical uncertainty in parameters is obtained as follows:

$$\mathrm{Var}\,[X_1] \simeq \frac{\pi}{4M^2\zeta\omega_n^3} G_1(\omega_n). \tag{5.36}$$

Upon substituting Eqs. 5.16–17, 3.10, and after some algebraic manipulations:

$$\mathrm{Var}\,[X_1] \simeq a_2 \frac{k_r C_d^2}{\zeta \omega_n^{14/3}}, \tag{5.37}$$

where

$$a_2 = \left(\frac{\rho_a h b}{M}\right)^2 \left(\frac{2\pi^4 \bar{V}_{10}^{13}}{L}\right)^{1/3}$$

is a deterministic quantity. Since the uncertain parameters such as k_r, C_d, ζ, and ω_n on the right side of Eq. 5.37 take only positive values, and invoking the central limit theorem, $\mathrm{Var}\,[X_1]$ may be modeled as a lognormal random variable. Thus,

$$\begin{aligned} \xi_1^2 &= \mathrm{Var}\,[\log(\mathrm{Var}\,[X_1])] \\ &= \xi_{k_r}^2 + 4\xi_{C_d}^2 + \xi_\zeta^2 + (\tfrac{14}{3})^2 \xi_{\omega_n}^2. \end{aligned} \tag{5.38}$$

5.2.2.2 Wave Drag

The sea-waves act on the structure along its height, over which the response, e.g., the relative displacement, varies. To calculate the modal load, therefore, only a fraction f of the

wave drag and wave inertia loads are lumped to the total load at the deck level. Assuming a triangular profile, a conservative choice, for the wave force over the height of the structure, factor f through modal analysis [16] is found to be 0.55.

Following Eq. 3.20, the drag force due to waves, P_2, integrated over the submerged depth of the legs becomes:

$$\begin{aligned} P_2 &= f \int_0^d \frac{1}{2} N C_d \rho_w D |u(z,t)| u(z,t) \\ &= f \int_0^d \frac{1}{2} N C_d \rho_w D \sqrt{8/\pi}\, \sigma_{u(z)} u(z,t)\, dz. \end{aligned} \tag{5.39}$$

The variance of water particle velocity, $\sigma^2_{u(z)}$, is related to the variance of wave height, σ^2_H, see Eq. 3.12:

$$\sigma^2_{u(z)} = \left(\frac{\omega}{2} \frac{\cosh kz}{\sinh kd} \right)^2 \sigma^2_H, \tag{5.40}$$

where σ_H can be obtained from Eq. 3.11 as the root of the area below the wave height spectrum:

$$\sigma_H = \sqrt{\frac{\alpha}{\beta}} \frac{\bar{V}_{10}}{2g}. \tag{5.41}$$

Upon substituting Eqs. 5.40–41 into Eq. 5.39 and carrying out the integration:

$$P_2 = f \frac{1}{\sqrt{32\pi}} N C_d \rho_w D \sqrt{\frac{\alpha}{\beta}} \frac{\bar{V}^2_{10}}{2g} \omega^2 \frac{d + (2k)^{-1} \sinh 2kd}{\sinh^2 kd} H \sin \omega t. \tag{5.42}$$

The SDF of wave drag, $G_2(\omega)$, then is written as

$$G_2(\omega) = T_2^2 G_H(\omega), \tag{5.43}$$

in which $G_H(\omega)$ is given by Eq. 3.11 and T_2, conditional on $\bar{V}_{10}$, is

$$T_2 = f \frac{1}{\sqrt{32\pi}} N C_d \rho_w D \sqrt{\frac{\alpha}{\beta}} \frac{\bar{V}^2_{10}}{2g} \omega^2 \frac{d + (2k)^{-1} \sinh 2kd}{\sinh^2 kd}. \tag{5.44}$$

Denoting the relative displacement response to wave drag as X_2,

$$G_{X_2} = |H(\omega)|^2 G_2(\omega). \tag{5.45}$$

Also, the variance of X_2 is obtained as the area below its SDF:

$$\mathrm{Var}\,[X_2] = \int_0^\infty G_{X_2}(\omega)\, d\omega. \tag{5.46}$$

Again, since $G_{X_2}(\omega)$ contains uncertain parameters, $\mathrm{Var}[X_2]$ is seen as a random variable. The mean of $\mathrm{Var}[X_2]$, denoted as $\sigma^2_{X_2,R}$, is approximated by evaluating the integral (5.46) with the mean values substituted for the uncertain parameters, and the variance of $\mathrm{Var}[X_2]$ is obtained as follows:

$$\begin{aligned}\mathrm{Var}[X_2] &\simeq \frac{\pi}{4M^2\zeta\omega_n^3} G_2(\omega_n) \\ &= a_3 \frac{\alpha^2 C_d^2}{\zeta\beta\omega_n^4} f_3,\end{aligned} \tag{4.47}$$

where

$$f_3 = \exp\left[-\left(\frac{g}{\bar{V}_{10}}\right)^4 \frac{\beta}{\omega_n^4}\right]$$

is a deterministic quantity. As argued before, since the uncertain parameters on the right side of Eq. 5.47 are all positive, $\mathrm{Var}[X_2]$ is seen as a lognormal random variable. Thus,

$$\begin{aligned}\xi_2^2 &= \mathrm{Var}[\log(\mathrm{Var}[X_2])] \\ &= 4\xi_\alpha^2 + 4\xi_{C_d}^2 + \xi_\zeta^2 + \xi_\beta^2 + 16\xi_{\omega_n}^2 + \xi_{f_3}^2.\end{aligned} \tag{5.48}$$

5.2.2.3 Wave Inertia

Following Eq 3.20, the inertia force due to waves, P_3, integrated over the submerged depth of the legs becomes:

$$\begin{aligned}P_3 &= fNC_m\rho_w \frac{\pi D^2}{4} \int_0^d \dot{u}(z,t)\, dz \\ &= fNC_m\rho_w \frac{\pi D^2}{4} \frac{\omega^2 H}{2} \frac{1}{\sinh kd} \sin\omega t \int_0^d \cosh kz\, dz \\ &= f\frac{\pi}{8} NC_m\rho_w D^2 \frac{\omega^2}{k} H \sin\omega t.\end{aligned} \tag{5.49}$$

The SDF of wave inertia, $G_3(\omega)$, then is written as

$$G_3(\omega) = T_3^2 G_H(\omega), \tag{5.50}$$

where T_3 is

$$T_3 = f\frac{\pi}{8} NC_m\rho_w D^2 \frac{\omega^2}{k}. \tag{5.51}$$

Denoting the displacement response to wave inertia as X_3,

$$G_{X_3}(\omega) = |H(\omega)|^2 G_3(\omega). \tag{5.52}$$

The variance of X_3 is equal to the area below its SDF:

$$\mathrm{Var}\,[X_3] = \int_0^\infty G_{X_3}(\omega)\, d\omega. \tag{5.53}$$

Here too, $G_{X_3}(\omega)$ contains uncertain parameters and hence $\mathrm{Var}\,[X_3]$ is seen as a random variable. The mean of $\mathrm{Var}\,[X_3]$, denoted as $\sigma^2_{X_3,R}$, is obtained by evaluating the integral (5.53) with the mean values substituted for the uncertain parameters, and the variance of $\mathrm{Var}\,[X_3]$ is obtained as follows:

$$\begin{aligned} \mathrm{Var}\,[X_3] &\simeq \frac{\pi}{4M^2\zeta\omega_n^3} G_3(\omega_n) \\ &= a_3 \frac{\alpha C_m^2}{\zeta\omega_n^4} f_3, \end{aligned} \tag{5.54}$$

where a_3 = deterministic quantity. As we argued before, since the uncertain parameters on the right side of Eq. 5.54 are all positive, and invoking the central limit theorem, $\mathrm{Var}\,[X_3]$ may be modeled as a lognormal random variable. Thus,

$$\begin{aligned} \xi_3^2 &= \mathrm{Var}\,[\log(\mathrm{Var}\,[X_3])] \\ &= \xi_\alpha^2 + 4\xi_{C_m}^2 + \xi_\zeta^2 + 16\xi_{\omega_n}^2 + \xi_{f_2}^2. \end{aligned} \tag{5.55}$$

5.2.2.4 Total Dynamic Response

The total dynamic response, denoted as X_d, is the sum of responses to wind drag, wave drag, and wave inertia:

$$X_d = X_1 + X_2 + X_3. \tag{5.56}$$

The variance of X_d, conditional on the mean wind velocity $\bar{V}_{10}$, is obtained by summing the variance contributions:

$$\mathrm{Var}\,[X_d] = \mathrm{Var}\,[X_1] + \mathrm{Var}\,[X_2] + \mathrm{Var}\,[X_3]\,. \tag{5.57}$$

5.2.2.5 Peak Response

The peak value of the combined dynamic response process can be written as

$$X_p = Z(\mathrm{Var}\,[X_d])^{1/2}, \tag{5.58}$$

in which Z is a random peak factor, see Eqs. 5.9–10. Making use of the Eqs. 5.58–59, statistics of random peak factor Z, and variances of X_1, X_2, X_3, we obtain the first two moments of X_p as presented below:

$$m_{X_p} = m_Z[\sigma^2_{X_1,R}\exp(-\xi_1^2/4) + \sigma^2_{X_2,R}\exp(-\xi_2^2/4) + \sigma^2_{X_3,R}\exp(-\xi_3^2/4)]^{1/2}. \tag{5.59}$$

$$\sigma^2_{X_p,U} = \sigma^2_Z(\sigma^2_{X_1,R} + \sigma^2_{X_2,R} + \sigma^2_{X_3,R}). \tag{5.60}$$

$$\begin{aligned}\sigma^2_{X_p,U} = m^2_Z\{&\sigma^2_{X_1,R}[1 - \exp(-\xi_1^2/4)] + \sigma^2_{X_2,R}[1 - \exp(-\xi_2^2/4)] \\ &+ \sigma^2_{X_3,R}[1 - \exp(-\xi_3^2/4)]\}.\end{aligned} \tag{5.61}$$

For the purpose of risk analysis, a quantity of central interest is the conditional peak of the total load-effect, denoted here as L_v, which is the sum of the static response and the peak dynamic response. The subscript v indicates the response dependence on the wind intensity. Thus,

$$m_{L_v} = m_{X_s} + m_{X_p}. \tag{5.62}$$

$$\sigma^2_{L_v} = \sigma^2_{X_s,U} + \sigma^2_{X_p,R} + \sigma^2_{X_p,U}. \tag{5.63}$$

5.3 Response to Earthquake Load Plus Sea-storm Load

When an earthquake and a sea-storm coincide, the responses to earthquake, wind, wave, and current loads may be superimposed. The short-duration combined response then has a static component due to wind and current loads, and a dynamic component due to earthquake, wind and wave loads. To obtain the peak response, we calculate the peak dynamic response and add to it the static response. The peak dynamic response is obtained by adding the individual response variances and then multiplying the root of the total variance by a random peak factor, dependent on the earthquake's event duration.

Let Y_s be the static displacement, X_s the static displacement due to wind and current loads (Eq. 5.26), Y_d the dynamic displacement, and Y_p the peak dynamic displacement. Then,

$$Y_s = X_s, \tag{5.64}$$

and

$$Y_d = X_1 + X_2 + X_3 + X_e, \tag{5.65}$$

where X_1, X_2, X_3, and X_e denote the dynamic displacements due to wind drag, wave drag, wave inertia, and earthquake loads, respectively. Thus,

$$Y_p = Z(\mathrm{Var}\,[Y_d])^{1/2}. \tag{5.66}$$

The first two moments of Y_p are given below:

$$m_{Y_p} = m_Z[\sigma^2_{X_1,R}\exp(-\xi_1^2/4) + \sigma^2_{X_2,R}\exp(-\xi_2^2/4) + \sigma^2_{X_3,R}\exp(-\xi_3^2/4)]^{1/2} + \sigma^2_{X_e,R}\exp(-\xi_e^2/4)]^{1/2}. \tag{5.67}$$

$$\sigma^2_{X_p,U} = \sigma^2_Z(\sigma^2_{X_1,R} + \sigma^2_{X_2,R} + \sigma^2_{X_3,R} + \sigma^2_{X_e,R}). \tag{5.68}$$

$$\sigma^2_{X_p,U} = m^2_Z\{\sigma^2_{X_1,R}[1 - \exp(-\xi_1^2/4)] + \sigma^2_{X_2,R}[1 - \exp(-\xi_2^2/4)] + \sigma^2_{X_3,R}[1 - \exp(-\xi_3^2/4)] + \sigma^2_{X_e,R}[1 - \exp(-\xi_e^2/4)]\}. \tag{5.69}$$

Let the conditional total peak response be denoted as L_{av}, where the subscript indicates the response dependence on the earthquake and sea-storm intensities, A and V, respectively. We may write

$$m_{L_{av}} = m_{X_s} + m_{Y_p}. \tag{5.70}$$

$$\sigma^2_{L_{av}} = \sigma^2_{X_s,U} + \sigma^2_{Y_p,R} + \sigma^2_{Y_p,U}. \tag{5.71}$$

5.4 Response to Earthquake Load Plus Ambient Load

When shaken by an earthquake offshore structures in addition experience the ambient wind, wave, and current loads that arise from the ever-present wind over the sea. Due to the ambient load the structure's response developes a bias, e.g., the displacement response developes a non-zero mean in the direction of the mean wind (assuming the same direction for the sea currents).

This load combination is a special case of the previous one, where we now specify a nominal constant value for the wind intensity V. Denoting the total peak response as L_{a*}, where the subscript $a*$ indicates the response dependence on the earthquake intensity, A, and a nominal sea-storm intensity, the first two moments of L_{a*} are obtained from Eqs. 70–71, by substituting a nominal constant value for the mean wind.

6. Risk Assessment

6.1 Limit State

An important ingredient of risk analysis is the identification of limit states, i.e., states of undesirable structural behavior. The probabilities of structural failure are calculated with reference to different limit states. This report considers two limit states, both of the first passage type, defined, respectively, in terms of relative displacement and (pseudo) acceleration at the deck level of the structure. Since the structure is modeled as a linear 1-DOF system, either of the two limit states can represent the allowable force, however, both cover some distinct aspects of structural behavior: the displacement limit state may also represent serviceability, i.e., the allowable displacement at the deck level; and, the acceleration limit state is pertinent to assessing the safety of secondary systems or acceleration-sensitive instruments mounted on the deck. The allowable limits, i.e., the resistances, are often random; they are modeled herein as lognormally distributed random variables, but with constant coefficient of variation, set at 0.25. The structural performance is assessed with several values for the mean resistance.

6.2 Risk Analysis

An offshore structure during its design life is subjected to intermittent loads due to earthquakes and sea-storms. The intensities of these loads, their occurrence patterns, the load parameters, the dynamic characteristics of the structure, and the structural resistance are all uncertain. Some of these, for example, the intensities and the occurrence patterns of the loads are inherently random, while others are statistically uncertain. To quantify the performance of the structure in this uncertain environment involves calculating the probabilities of structural failure during a prescribed period of time $(0\text{–}t)$. The following format has been adopted herein to calculate the failure probabilities.

First we calculate the "conditional failure probability," $p_{f|q,r}$, defined as the probability of structural failure given that a load event of intensity q occurs and that the structural resistance is r. The parameter q for a coincidental load event is a vector, i.e., $q = av$ for the event of simultaneous occurrence of earthquake and sea-storm. Also, the structural resistance

r, in general, is statistically uncertain and may degrade with time. The failure probability, therefore, needs to be convolved with the distribution of R, the uncertain resistance, at an appropriate stage of risk analysis. Recall that this report treats various other load and structural parameters as random variables too, which, in effect, renders the response statistics to be uncertain. For example, the stationary response variance to the earthquake load was seen in section five to be random and lognormally distributed, with the variability attributed to the uncertain parameters. There are several ways one can account for this additional uncertainty in a risk analysis. This report adopts an approach whereby we calculate the statistics of the peak load-effect, L_q, due to the individual and coincidental load events, and assume that the peak load-effects are lognormally distributed. The mean and the variance of L_q include the effect of uncertainty in the load and structural parameters. In other approach, for example, the barrier crossing approach [12,14], one may first calculate the conditional failure probability, $p_{f|q,r,u}$, where the additional subscript u indicates the response dependence on a vector of uncertain parametrs, U, and then from it obtain $p_{f|q,r}$ by convolution.

The conditional failure probability, $p_{f|q,r}$, for a lognormal conditional load-effect, L_q, is calculated as

$$\begin{aligned} p_{f|q,r} &= P[L_q > r] \\ &= \Phi(-\beta_q), \end{aligned} \tag{6.1}$$

where

$$\beta_q = -\frac{\ln \mu_q}{\sqrt{\ln(1+V_{L_q}^2)}},$$

$$\mu_q = r/m_{L_q}\sqrt{1+V_{L_q}^2},$$

V_{L_q} = the coefficient of variation of L_q, and $\Phi(.)$ = the probability function of a standard normal variable. The index β_q is a conditional reliability index directly related to the conditional failure probability.

The "conditional failure probability per event," $p_{f|r}$, given that an event occurs (the event intensity is now random) and that the structural resistance is r, is then obtained by convolving $p_{f|q,r}$ with the distribution of the intensity parameter Q:

$$p_{f|r} = \int p_{f|q,r}\, f_Q(q)\, dq. \tag{6.2}$$

In a long-term risk analysis, we consider only those load events that exceed certain thresholds on the load-event-intensities. This report sets 20 gal for the peak ground acceleration of earthquake load events and 36 km per hour for the mean wind velocity of sea-storm load events, respectively, as the thresholds. The criterion for adopting these values is that the contribution of the load events with lower intensities to the failure probabilities per event are negligible. Setting the thresholds also gives the mean yearly event-occurrence rates, see Eq. 3.9, and the normalized intensity distribution functions to be used in the convolution in Eq. 6.2. The mean event-occurrence rates for earthquake and sea-storm are obtained through Eqs. 3.1, 3.8, and 3.9 as 0.5 per year and 1.0 per year, respectively.

The long-term or "overall" probability of structural failure due to a single intermittent load say in t years of service life is calculated as

$$p_{f,t} = 1 - \int (1 - p_{f|r})^N f_R(r)\, dr, \tag{6.3}$$

where N is the total number of load events in t years. If $p_{f|r}$ is small and the events occur as points in a Poisson process, Eq. (6.3) can be rewritten as

$$p_{f,t} = 1 - \int \exp(-\lambda t\, p_{f|r})\, f_R(r)\, dr, \tag{6.4}$$

where λ is the mean yearly event-occurrence rate of the load.

In the case of two independent, intermittent loads, there exist three kinds of load events: two individual load events and one coincidental load event. The overall failure probability, assuming Poisson arrivals for the the load events, then can be calculated as [15]:

$$p_{f,t} = 1 - \int \exp\left[-(\nu_1\, p_{1|r} + \nu_2\, p_{2|r} + \nu_{12}\, p_{12|r})t\right]\ f_R(r)\, dr, \tag{6.5}$$

where $p_{i|r}$ stands for '$p_{f|r}$' for the individual events of the ith load, $p_{12|r}$ that for the coincidental load, ν_i is the mean yearly event-occurrence rate of load i, and ν_{12} that of the coincidental load. For two independent loads with Poisson arrival:

$$\begin{aligned} \nu_i &= \lambda_i[1 - \sum_{i \neq j} \lambda_j (t_{01} + t_{02})], \\ \nu_{12} &= \lambda_1 \lambda_2 (t_{01} + t_{02}), \end{aligned} \tag{6.6}$$

in which t_{0i} is the event duration of load i.

If the failure probabilities $p_{i|r}$ and $p_{12|r}$ are very small, if the load events are rare, or if the variability in the structural resistance is small, one may convolve $p_{i|r}$ and $p_{12|r}$ individually with the distribution of the uncertain resistance, R, to obtain the unconditional failure probabilities per events of the individual and coincidental loads, respectively:

$$p_i = \int p_{i|r}\, f_R(r)\, dr; \tag{6.7}$$

$$p_{12} = \int p_{12|r}\, f_R(r)\, dr.$$

We may then rewrite Eqs. 6.4 and 6.5, respectively, as

$$p_{f,t} = 1 - \exp(-\lambda t\, p_f), \tag{6.4a}$$

and

$$p_{f,t} = 1 - \exp\left[-(\nu_1\, p_1 + \nu_2\, p_2 + \nu_{12}\, p_{12})t\right]. \tag{6.5a}$$

However, doing so amounts to assuming that the structural resistance from event to event is independent, and also ignores the fact that the combined load-effect and not the individual load-effect see the variability in the resistance. As a result, Eqs. 6.4a and 6.5a would always yield conservative estimates for the long-term failure probabilities. In the next section, we show several numerical results to substantiate this point.

The format of long-term risk assessment through Eqs. 6.4 and 6.5 is also easily amenable to include any degradation in the structural resistance over time.

The conditional failure probability per event against coincidental load, i.e., that due to the simultaneous occurrence of earthquake and sea-storm loads, is obtained by convolution:

$$\hat{p}_{12|r} = \int\int p_{12|av,r}\, dF_A(a)\, dF_V(v). \tag{6.8}$$

However, note that the event duration for an earthquake is only 20 sec as opposed to the assumed 20 minutes for a sea-storm alone. Thus, a coincidental load is invariably accompanied by a sea-storm load acting separately. Therefore, the conditional failure probability per event of a coincidental load, $p_{12|r}$, is the failure probability of a system with two failure events in series:

$$p_{12|r} = 1 - (1 - \hat{p}_{12|r})(1 - p_{2|r}), \tag{6.9}$$

where $p_{2|r}$ is the conditional failure probability per event against sea-storm loads.

7. Results

7.1 Conditional and Overall Failure Probabilities

In Fig. 7.1, we demonstrate the profound effect parameter uncertainty has on the response statistics. Shown in the figure are the probability density functions of resistance and peak response to a sea-storm load. The mean wind velocity of the sea-storm is 140 km/hr and the mean and the coefficient of variation (COV) of the resistance are 25 cm and 0.25, respectively. The figure shows that the presence of parameter uncertainty leads to a steep increase in the COV of the peak response: to 0.37 from 0.04; but a slight decrease in the mean: to 15 cm from 16 cm. A decrease in the mean occurs due to the lognormality of the stationary response variance, as shown in section five. It is interesting to note that the simultaneous occurrence of an increase in the COV of the peak response while a decrease in its mean may steer the conditional failure probability either way: an increase, or may be a decrease, depending on the load intensity and other parameters.

Figs. 7.2–7.8 show the probabilities of structural failure against earthquake load based on displacement limit state. In Fig. 7.2, we plot the conditional failure probability versus the peak ground acceleration when the allowable displacement at the deck level of the structure is 25 cm, both with and without the parameter uncertainty. Interestingly enough, the presence of parameter uncertainty leads to an increase in the conditional failure probability only when the peak ground acceleration is less than around 1.6 m/sec^2, a decrease otherwise. It indicates that if the contribution of events with peak ground acceleration less than 1.6 m/sec^2 outweigh the contribution of events with higher intensity to the conditional failure probability per event, the presence of parameter uncertainty will lead to an increase in the overall failure probability. In Fig. 7.3, we apportion the conditional failure probability per event, $p_{f|r}$, among the contributing peak ground accelerations. We see that most of the contribution to $p_{f|r}$ comes from earthquake-events with intensities around 1.5 m/sec^2. In Fig. 7.4, we plot $p_{f|r}$ versus resistance with and without the parameter uncertainty. The parameter uncertainty is seen to always increase the failure probability per event, though the increase is pronounced only at lower resistance levels. Fig. 7.5 shows the yearly failure probability versus the mean resistance calculated in two different ways. Recall that the structural resistance possesses statistical uncertainty, and at what stage of risk analysis the failure probability is convolved

with the distribution of resistance is important. The correct way to do it is to convolve the overall failure probability as shown in Eq. 6.4, because the structural resistance from event to event is the same, saving the possibility of degradation in the resistance. However, Eq. 6.4a, where we convolve the failure probability per event, is a reasonable approximation, though always conservative, if the failure probability is small. This figure and Fig. 7.7, where we plot the overall failure probability over 30 years of the service life of the structure, support this argument. Figs. 7.6 and 7.8 show the overall failure probabilities over one year and 30 years of service life, respectively, demonstrating the detrimental effect of the parameter uncertaity.

Figs. 7.9–7.13 show the similar results for the failure probabilities against earthquake load based on acceleration limit state. A major difference attributed to the acceleration limit state is that the effect of parameter uncertainty is less pronounced.

In Figs. 7.14 and 7.15, we plot the overall failure probabilities over 30 years of service life against earthquake load in the presence of the ambient vibration of three different intensities, based on displacement and acceleration limit states, respectively. It is seen that the ambient load leads to an increase in the failure probability, but perceptibly only at the lower resistance levels. The reason is that as the resistance level increases, so does the allowable response, which, in turn, diminishes the contribution of ambient vibration to the total response.

Figs. 7.16–7.20 show the failure probabilities against sea-storm loads based on displacement limit state. In Fig. 7.16, we plot the conditional failure probability versus the mean wind velocity when the resistance is 25 cm, both with and without the parameter uncertainty. The figure indicates that when the mean wind is less than around 45 m/sec, the presence of parameter uncertainty leads to an increase in the conditional failure probability. Fig. 7.17 shows the apportionment of the conditional failure probability per event among the mean wind velocities indicating that the storms with the mean wind around 40 m/sec contribute the most to the overall failure probability. Fig. 7.18 plots $p_{f|r}$ versus resistance with and without the parameter uncetainty. A comparison of Fig. 7.18 with Fig. 7.4, which is for the case of earthquake load, indicates that the effect of parameter uncertainty is more pronounced in the case of storm loads. The reason may be that relatively more number of parameters treated as uncertain go in to the response analysis in the case of storm load than for the earthquake load. Figs. 7.19 and 7.20 show the overall failure probability over 30 years of service life of the structure.

Figs. 7.21 to 7.25 show the failure probabilities against sea-storm load based on acceleration limit state. The results are dramatic. Both conditional and overall failure probabilities are seen to be exceedingly small. To put the results in perspective, recall that the mean natural period of the structure is 2.84 sec, far from the 25 sec period for the predominant wave. As a result, although storm loads induce large displacements, the acceleration response is small. This result is beneficial in that that acceleration-sensitive instruments or secondary systems mounted on the deck are not at risk during sea-storms; though, they might get blown off the deck.

In Fig. 7.26, based on displacement limit state, we plot the overall failure probabilities over 30 years for four different combinations of environmental loads, namely, earthquake load alone; earthquake load plus ambient load; sea-storm load alone; and earthquake load plus sea-storm load, with and without the load-coincidence. It is seen that the storm load governs the design, and the effect of coincidental load on the overall risk is negligible. Fig. 7.27 shows the 30-year-overall failure probability based on displacement limit state against both earthquake and storm loads acting on the structure, with and without the parameter uncertainty. The parameter uncertainty is seen to substantially increase the failure probability. Figs. 7.28–7.29 show the similar results in the case of acceleration limit state indicating that in this case the earthquake load governs the design, and the effect of parameter uncertainty is less important.

7.2 Sensitivity Analysis

The sensitivity of 30-year-overall failure probability against both earthquake and sea-storm loads acting on the structure has been investigated with reference to the mean and the coefficient of variation of the structure's natural frequency and the damping ratio. Figs. 7.30 and 7.31 show the results for the case of displacement limit state, while Figs. 7.32 and 7.33 for the case of acceleration limit state.

In Fig. 7.30a, we plot the 30-year-overall failure probability for three different values of mean natural frequency of the structure. As the structure becomes stiffer, due the displacement type limit state, the failure probability decreases. Fig. 7.30b shows the sensitivity of the failure probability to the variability in the natural frequency. It is apparent that the failure

probabilities are very sensitive to the variability in the natural frequency. Fig. 7.31 shows the sensitivity of 30-year-overall failure probability to the mean and the COV of the damping ratio. It is seen that the overall risk increases with the decrease in the mean damping and an increase in its variability.

In Fig. 7.32, based on acceleration limit state, we plot 30-year-overall failure probability for three different values of the mean natural frequency and three different values of its COV. The overall risk increases as the structure becomes stiffer, because of the acceleration type limit state. The overall risk in this case is less sensitive to the variability in the natural frequency. Fig. 7.33 shows similar result for the structure's damping ratio.

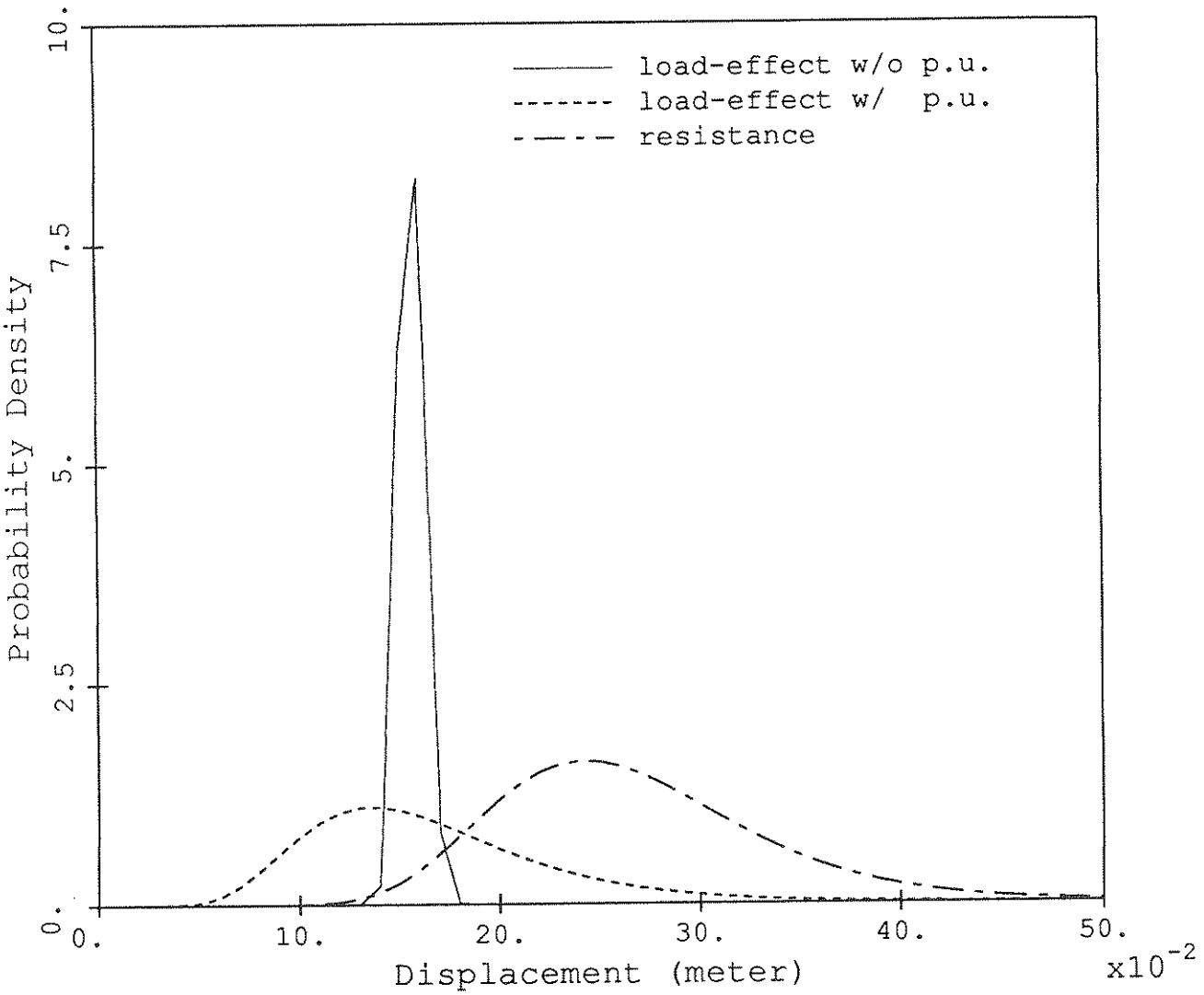

FIGURE 7-1 Probability Density Functions of Resistance and Peak Load-Effect in the Case of a Sea-Storm

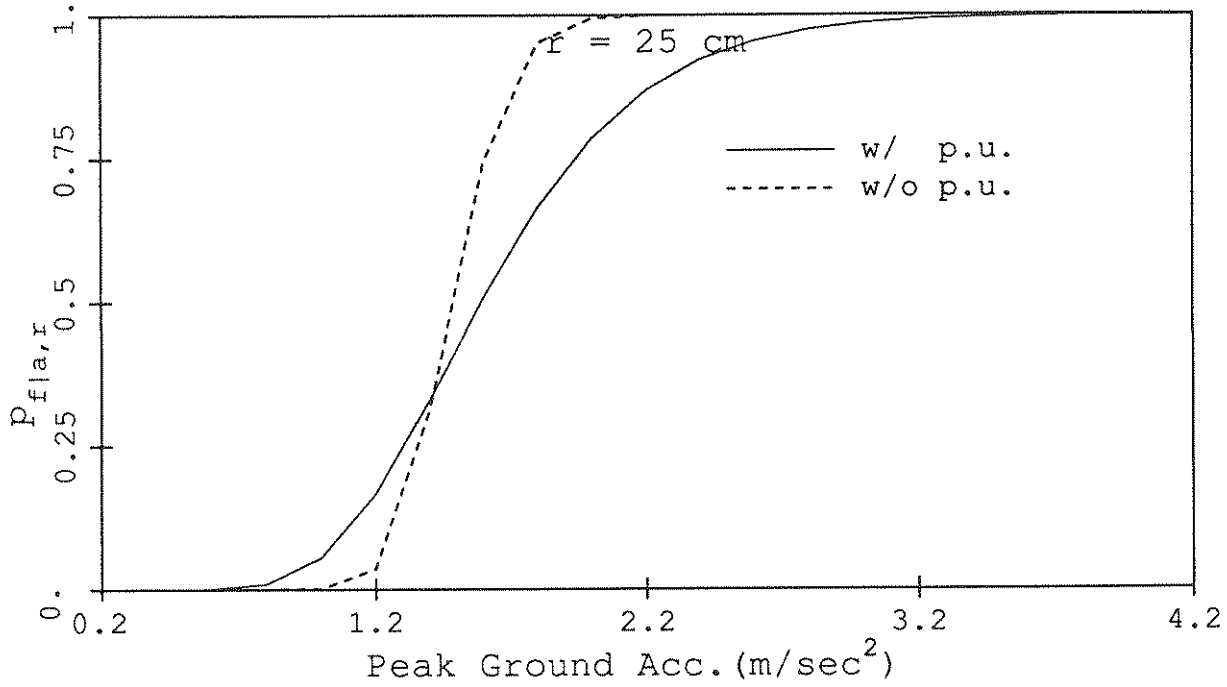

FIGURE 7-2 Conditional Failure Probability Against Earthquake Load Based on a Displacement Limit State

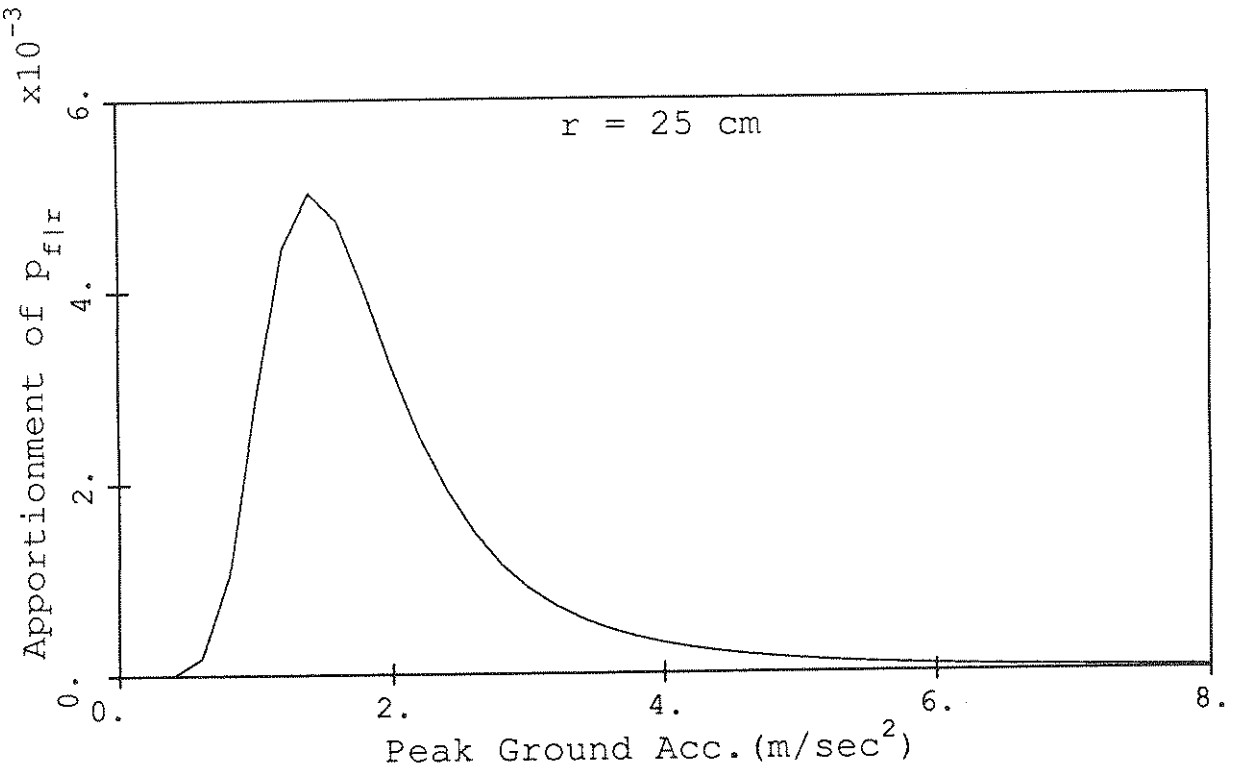

FIGURE 7-3 Conditional Failure Probability Per Event, Against Earthquake Load Based on a Displacement Limit State, Apportioned Among Peak Ground Accelerations

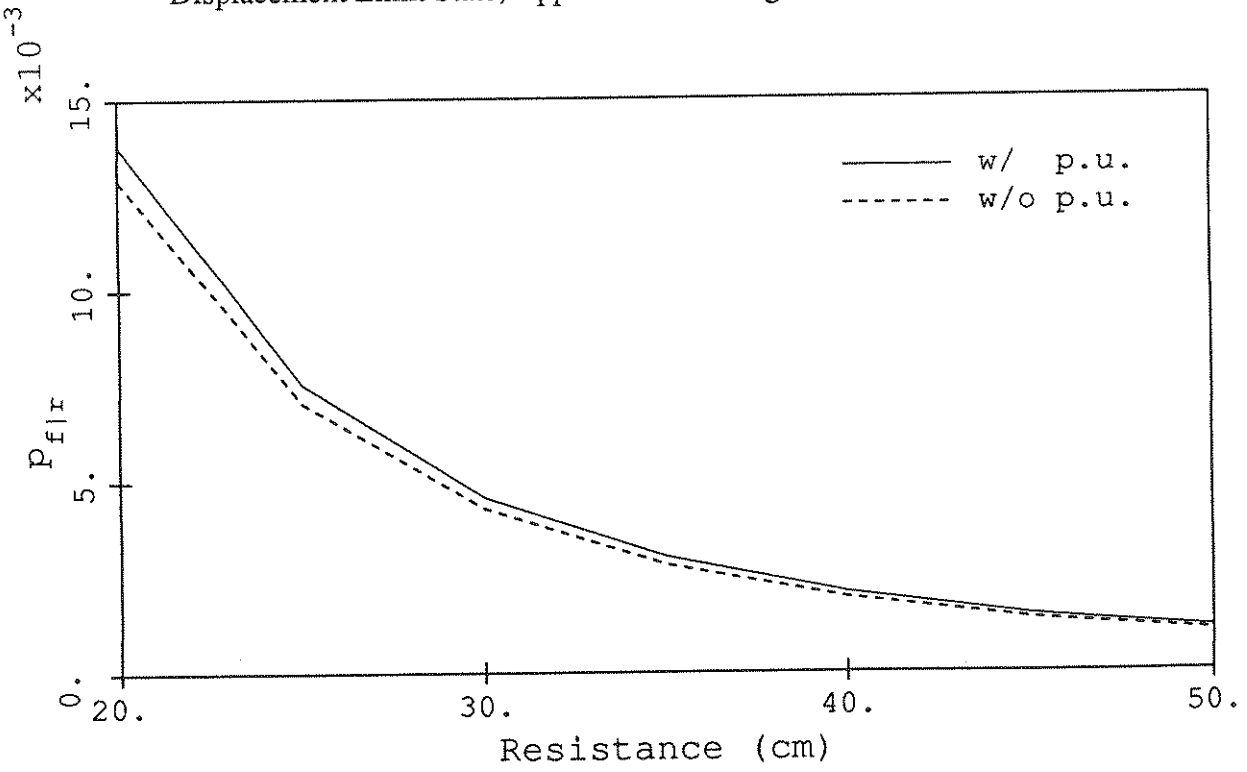

FIGURE 7-4 Conditional Failure Probability Per Event Against Earthquake Load Based on Displacement Limit State

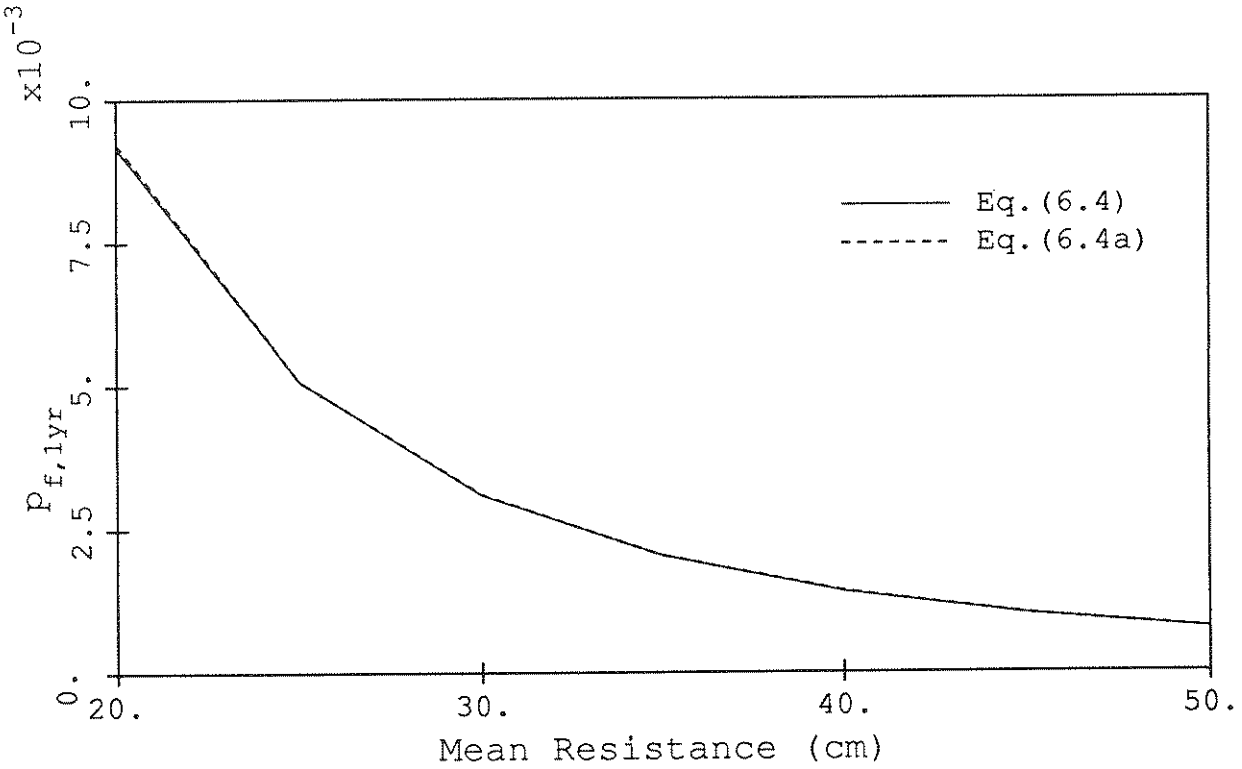

FIGURE 7-5 Overall Failure Probability in One Year Against Earthquake Load Based on Displacement Limit State

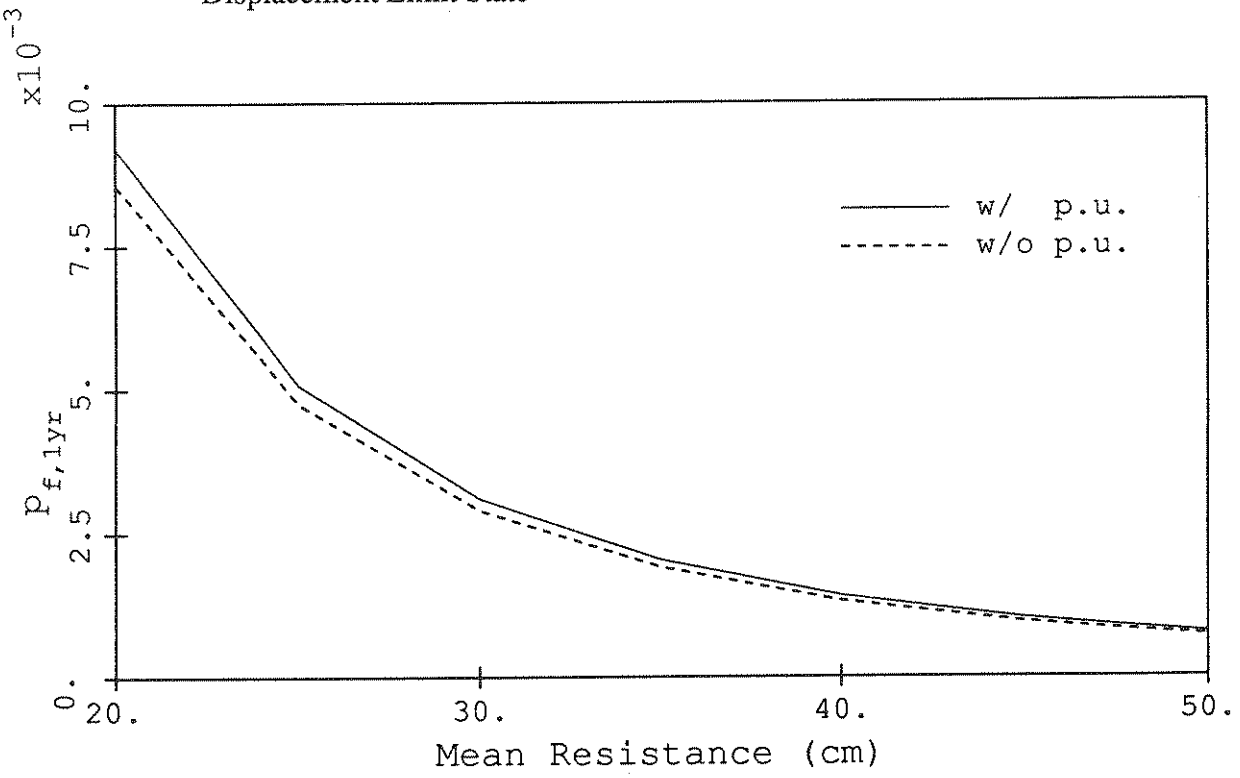

FIGURE 7-6 Overall Failure Probability in One Year Against Earthquake Load Based on Displacement Limit State, With and Without the Parameter Uncertainty

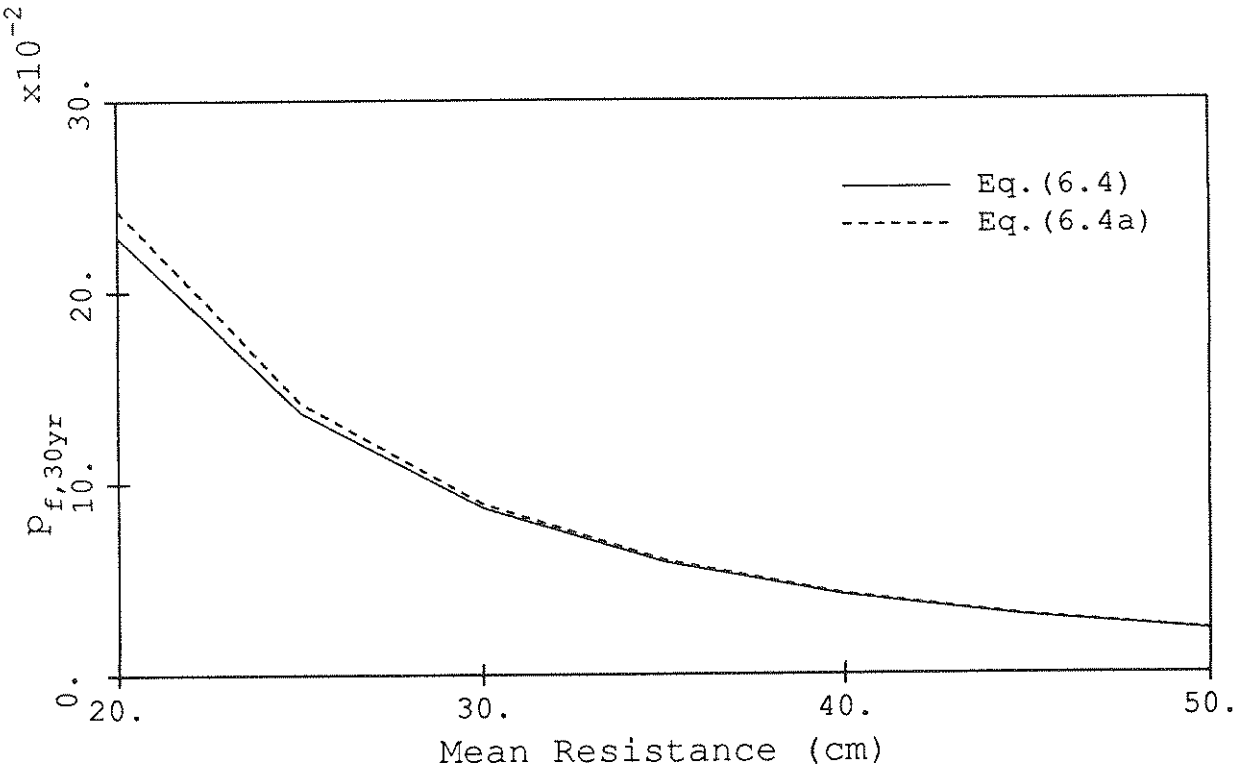

FIGURE 7-7 Overall Failure Probability in 30 Years Against Earthquake Load Based on Displacement Limit State

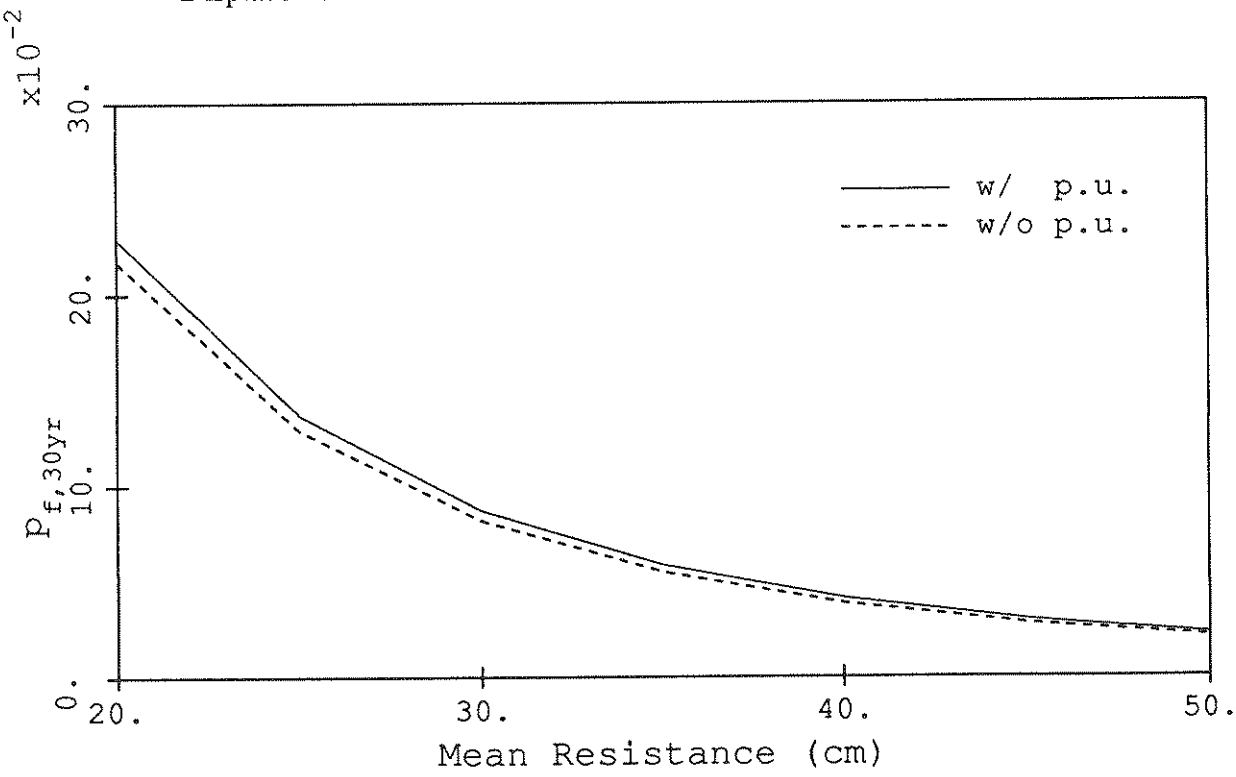

FIGURE 7-8 Overall Failure Probability in 30 Years Against Earthquake Load Based on Displacement Limit State, With and Without the Parameter Uncertainty

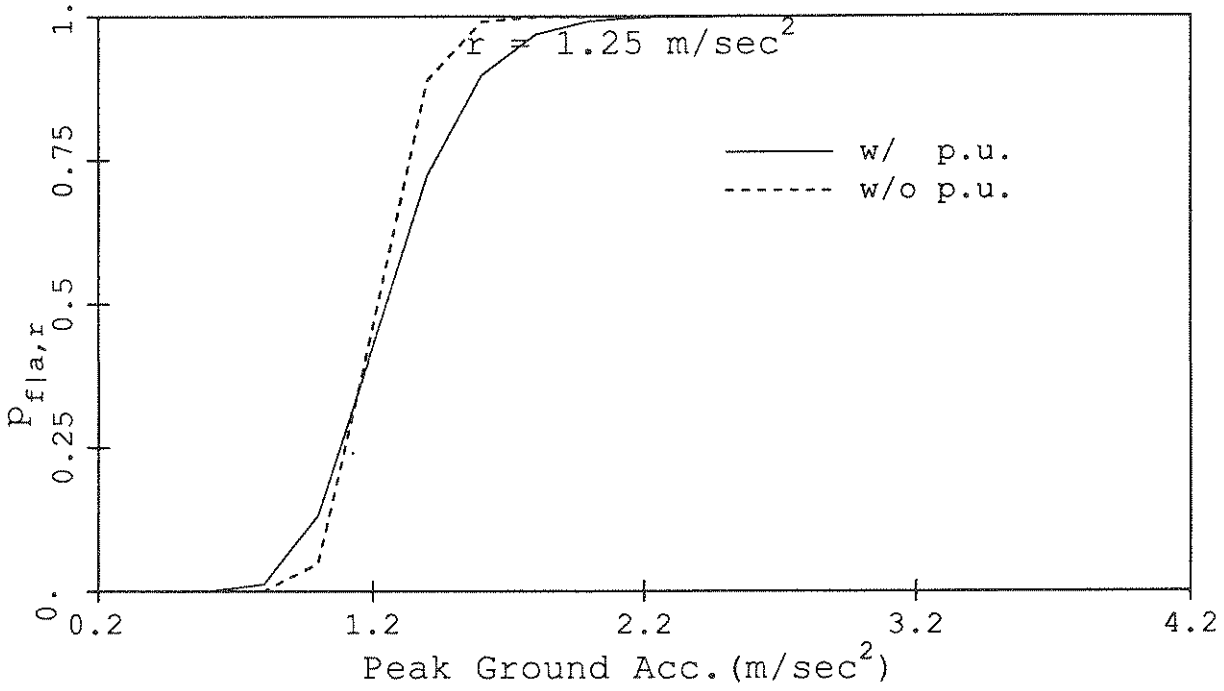

FIGURE 7-9 Conditional Failure Probability Against Earthquake Load Based on an Acceleration Limit State

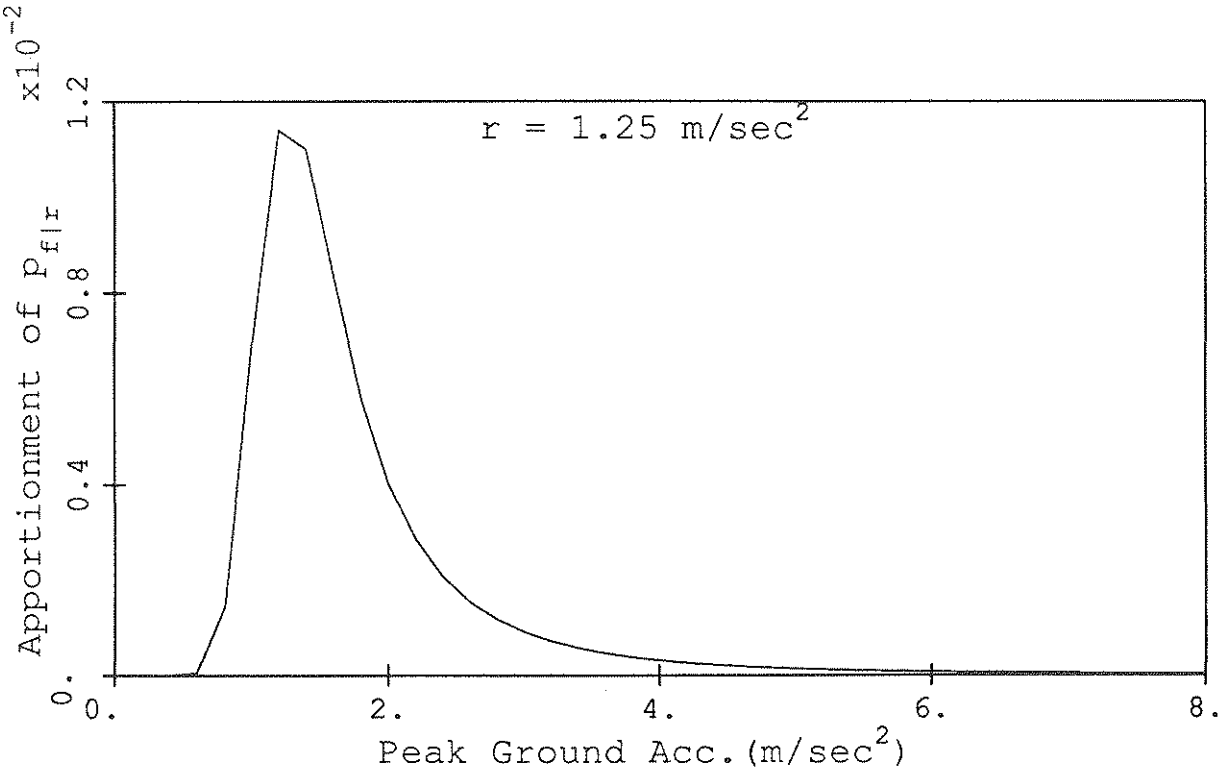

FIGURE 7-10 Conditional Failure Probability Per Event, Against Earthquake Load Based on an Acceleration Limit State, Apportioned Among Peak Ground Accelerations

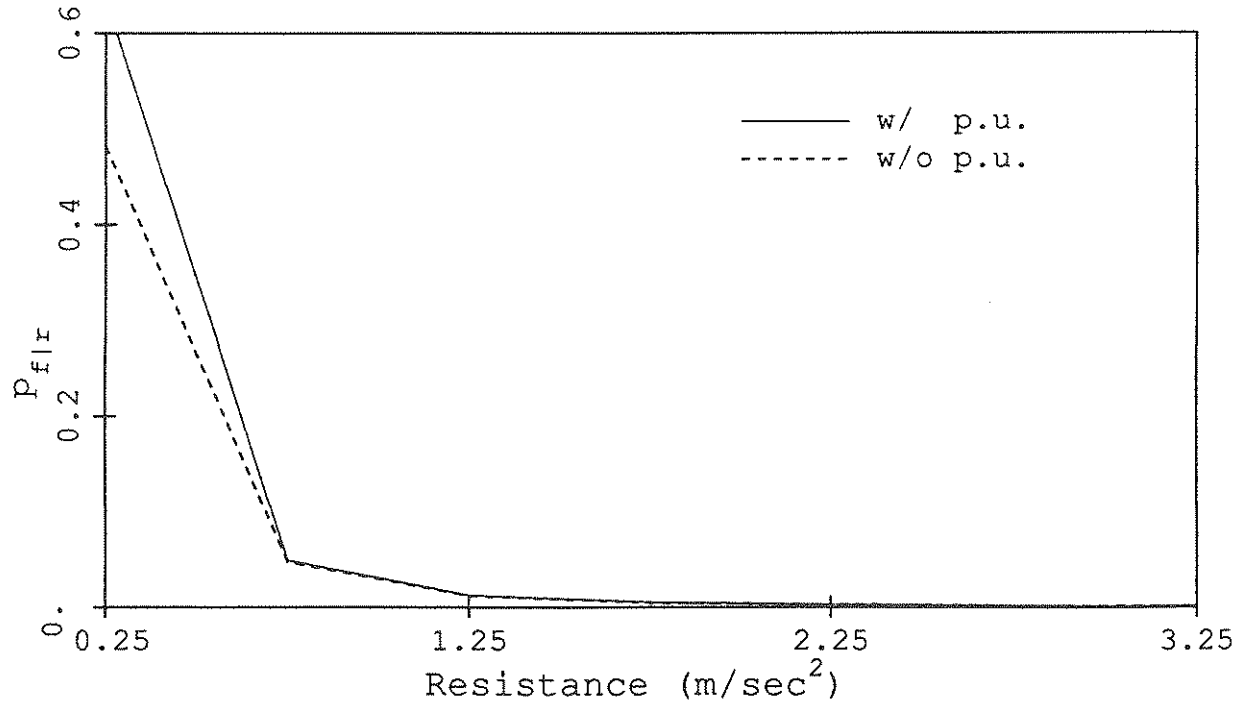

FIGURE 7-11 Conditional Failure Probability Per Event Against Earthquake Load Based on Displacement Limit State

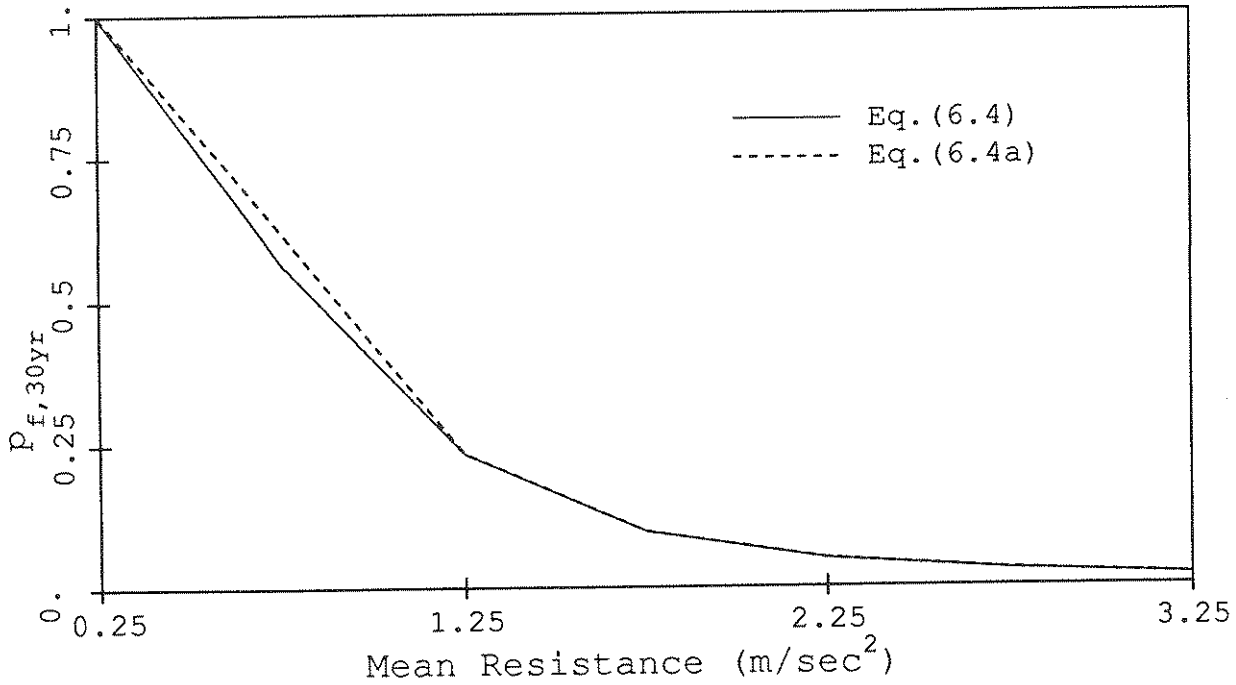

FIGURE 7-12 Overall Failure Probability in 30 Years Against Earthquake Load Based on Acceleration Limit State

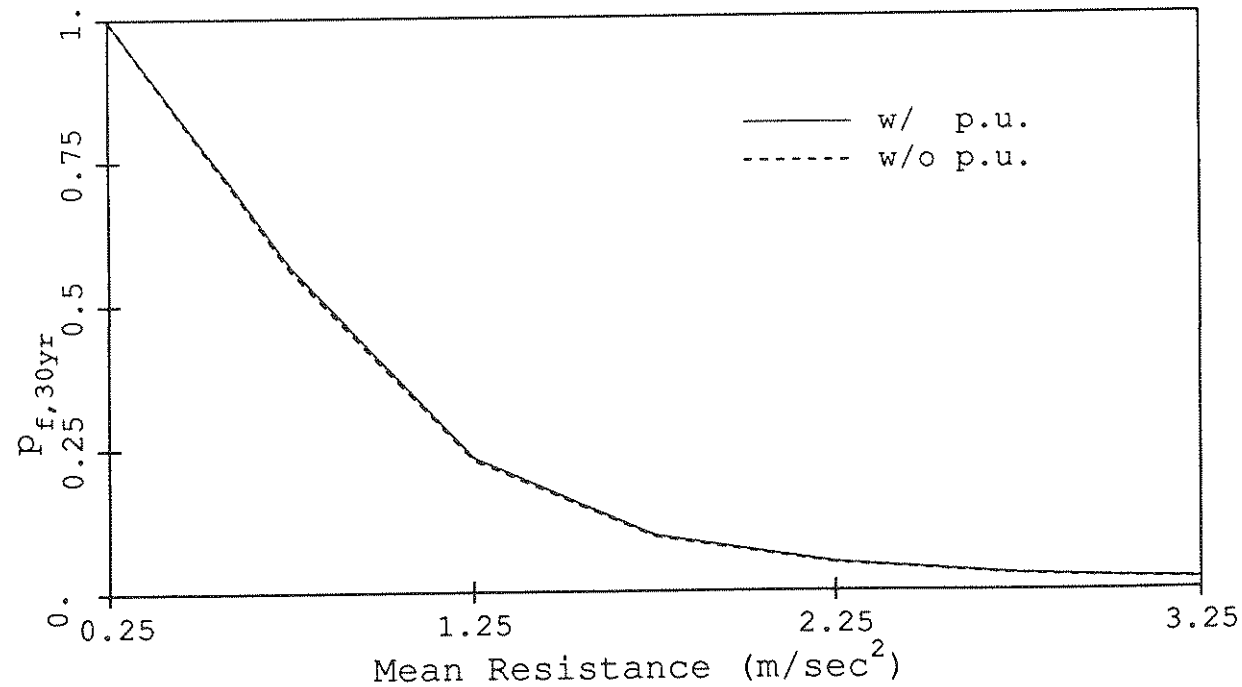

FIGURE 7-13 Overall Failure Probability in 30 Years Against Earthquake Load Based on Acceleration Limit State, With and Without the Parameter Uncertainty

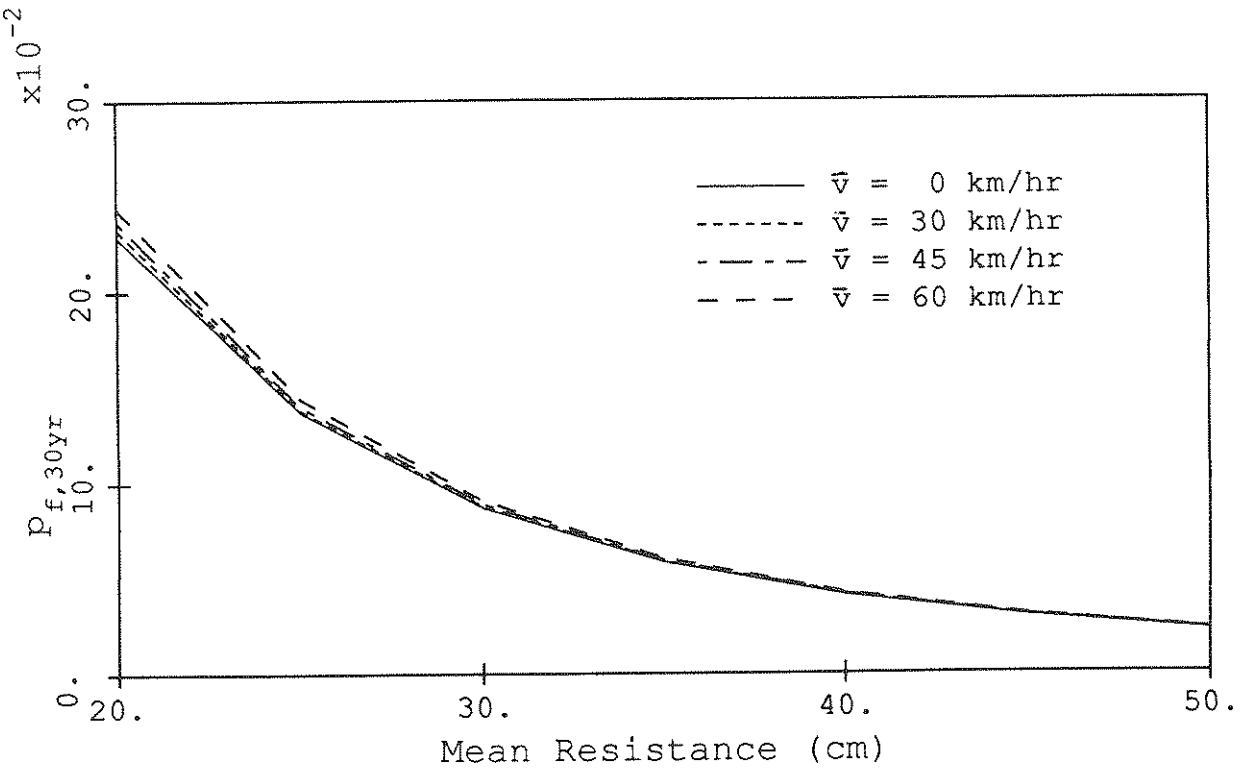

FIGURE 7-14 Overall Failure Probability in 30 Years Against Earthquake Load Plus Ambient Load Based on Displacement Limit State

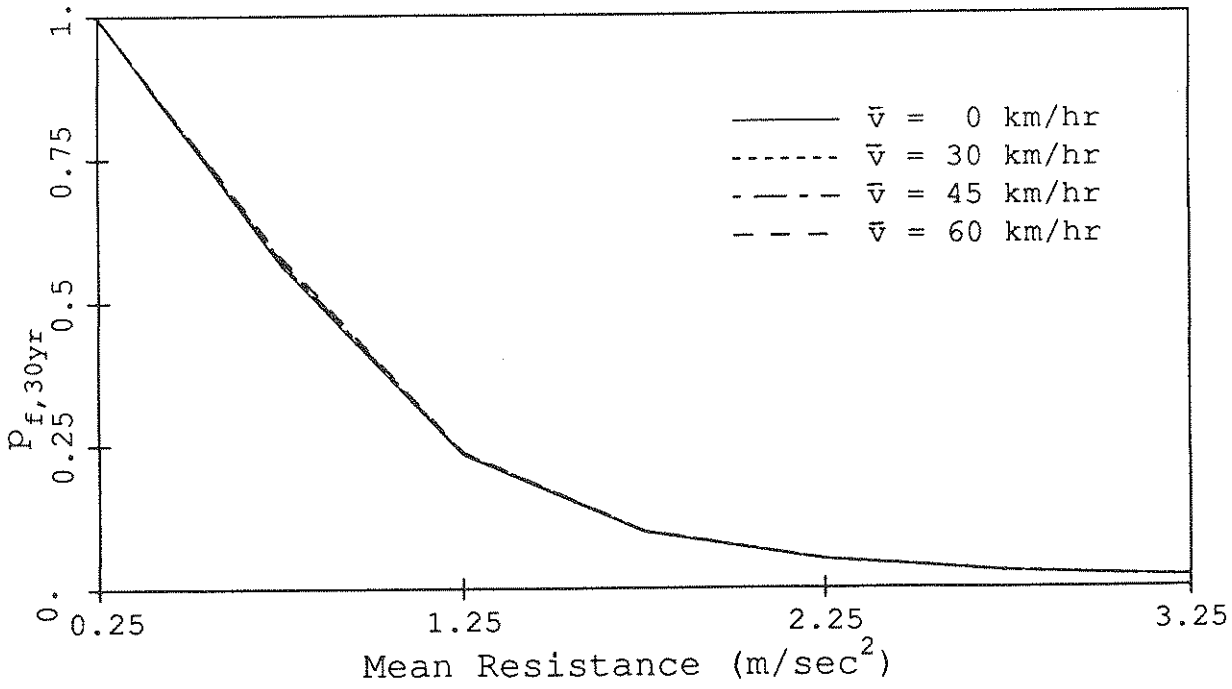

FIGURE 7-15 Overall Failure Probability in 30 Years Against Earthquake Load Plus Ambient Load Based on Acceleration Limit State

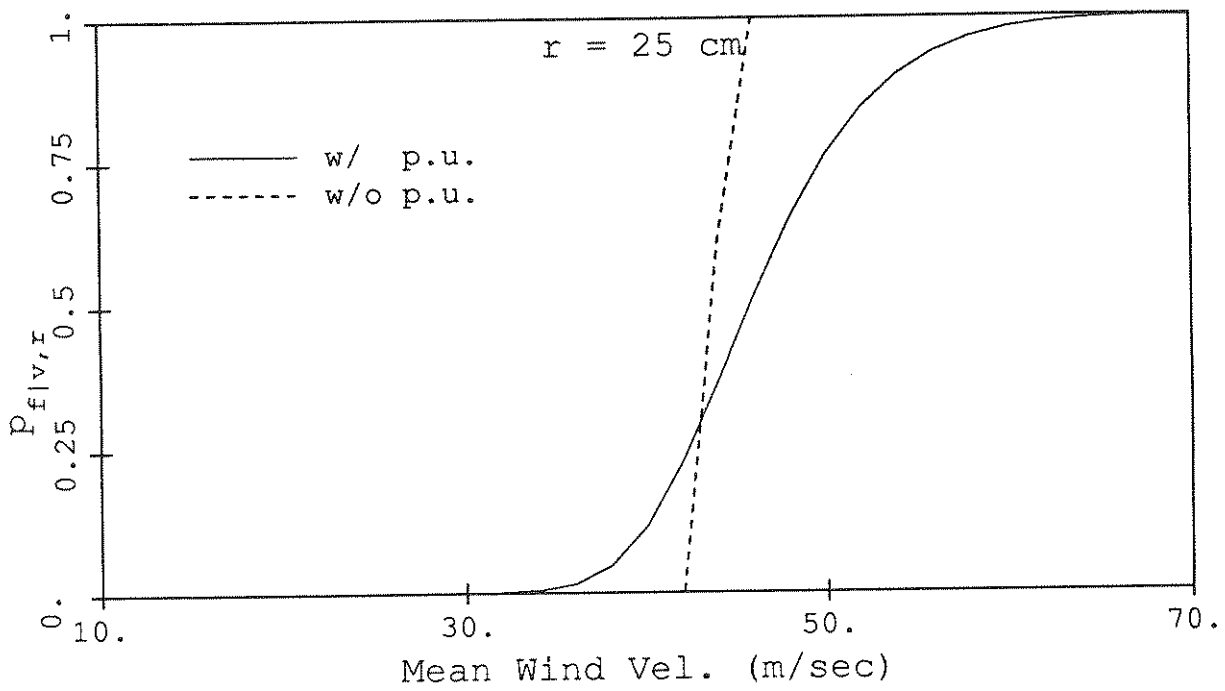

FIGURE 7-16 Conditional Failure Probability Against Sea-Storm Load Based on a Displacement Limit State

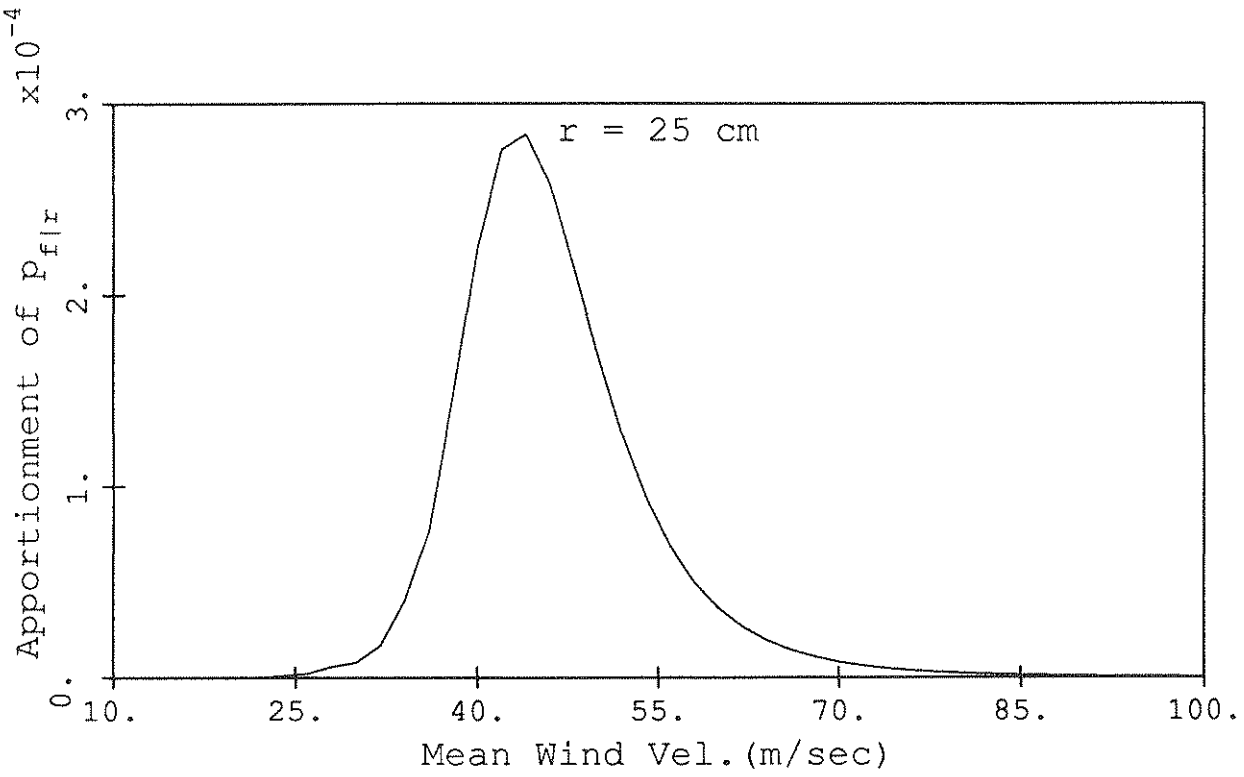

FIGURE 7-17 Conditional Failure Probability Per Event, Against Sea-Storm Load Based on a Displacement Limit State, Apportioned Among Mean Wind Velocities

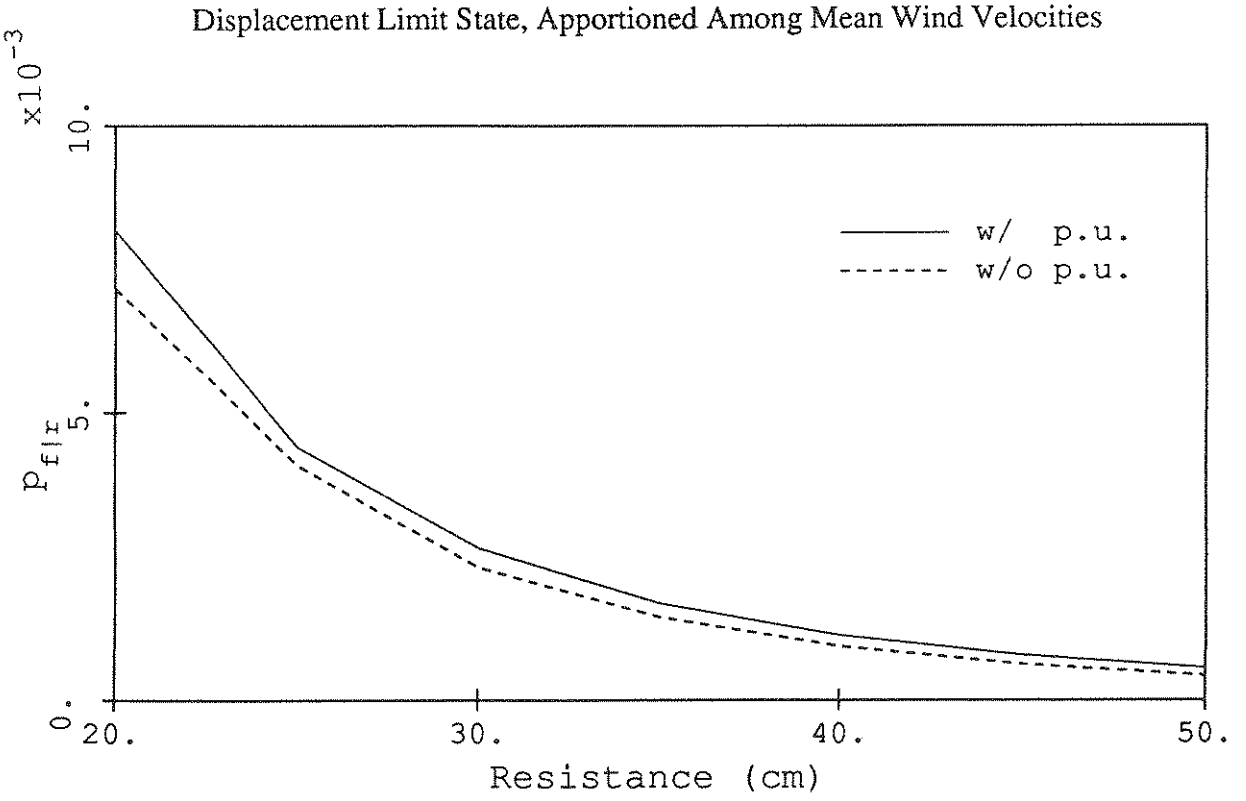

FIGURE 7-18 Conditional Failure Probability Per Event Against Sea-Storm Load Based on Displacement Limit State

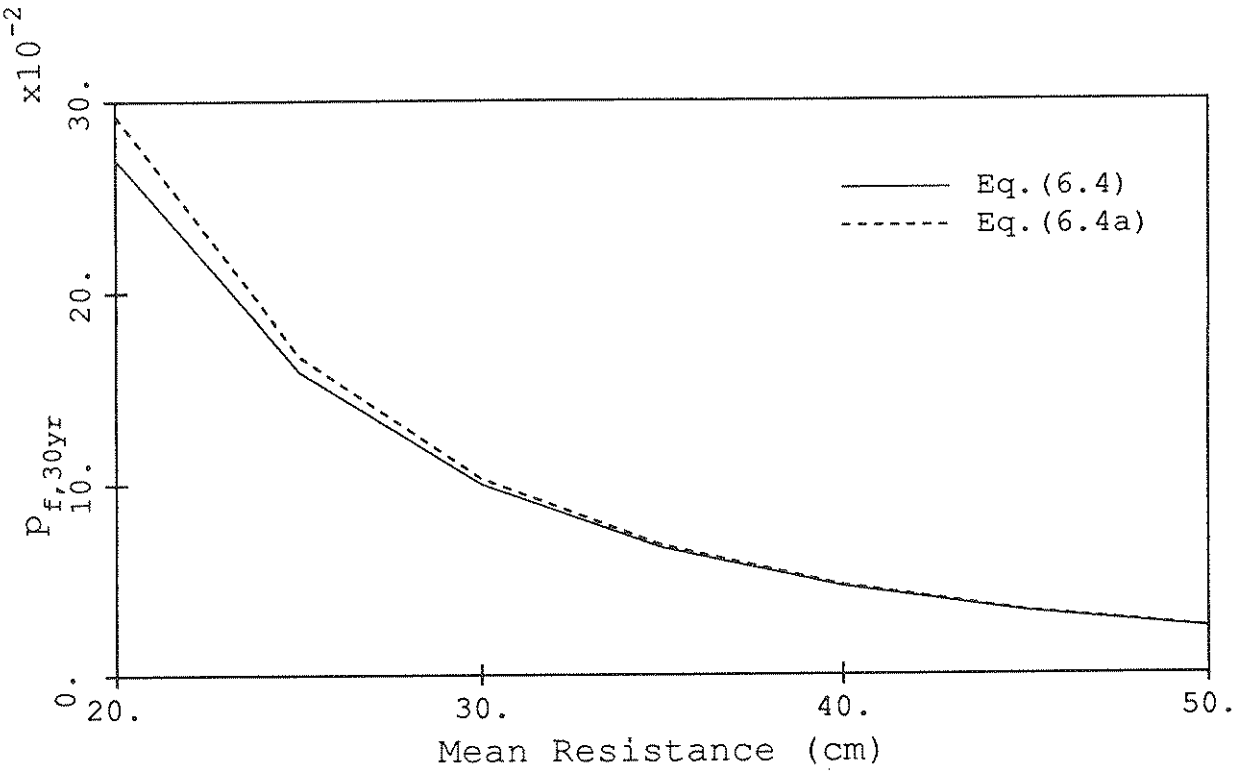

FIGURE 7-19 Overall Failure Probability in 30 Years Against Sea-Storm Load Based on Displacement Limit State

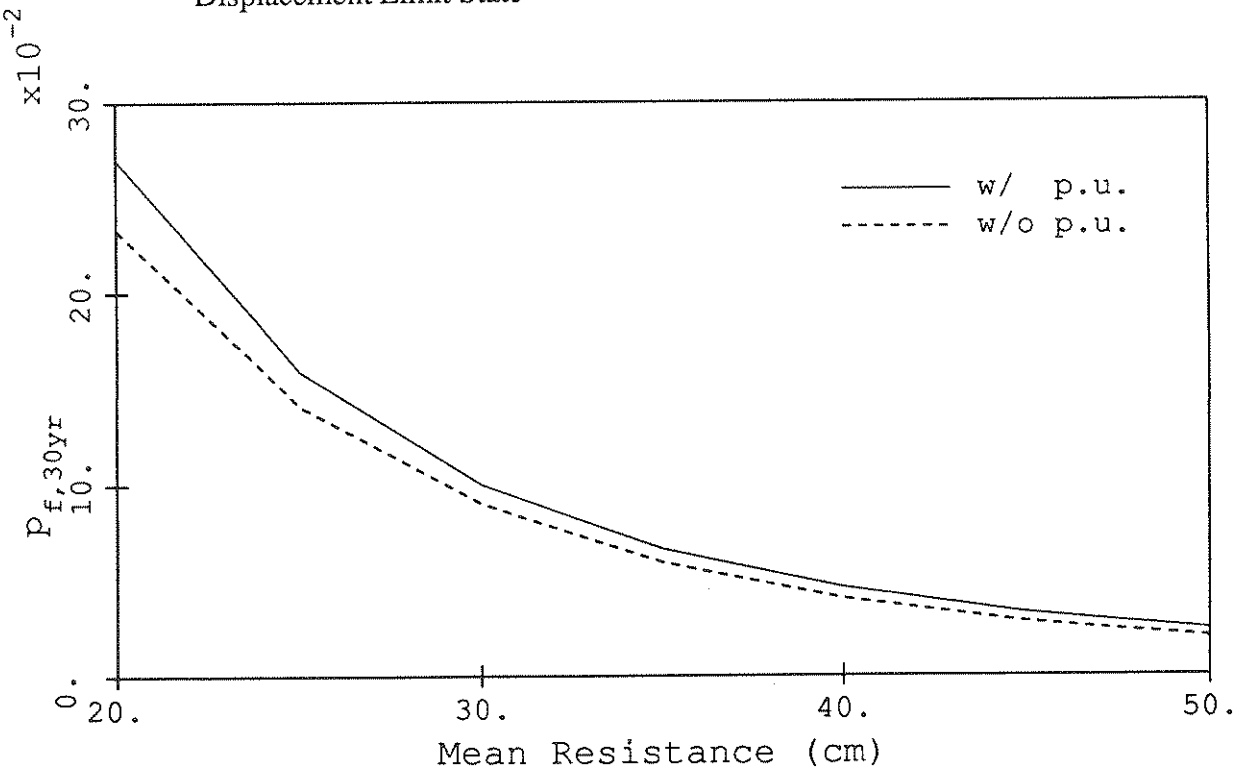

FIGURE 7-20 Overall Failure Probability in 30 Years Against Sea-Storm Load Based on Displacement Limit State, With and Without the Parameter Uncertainty

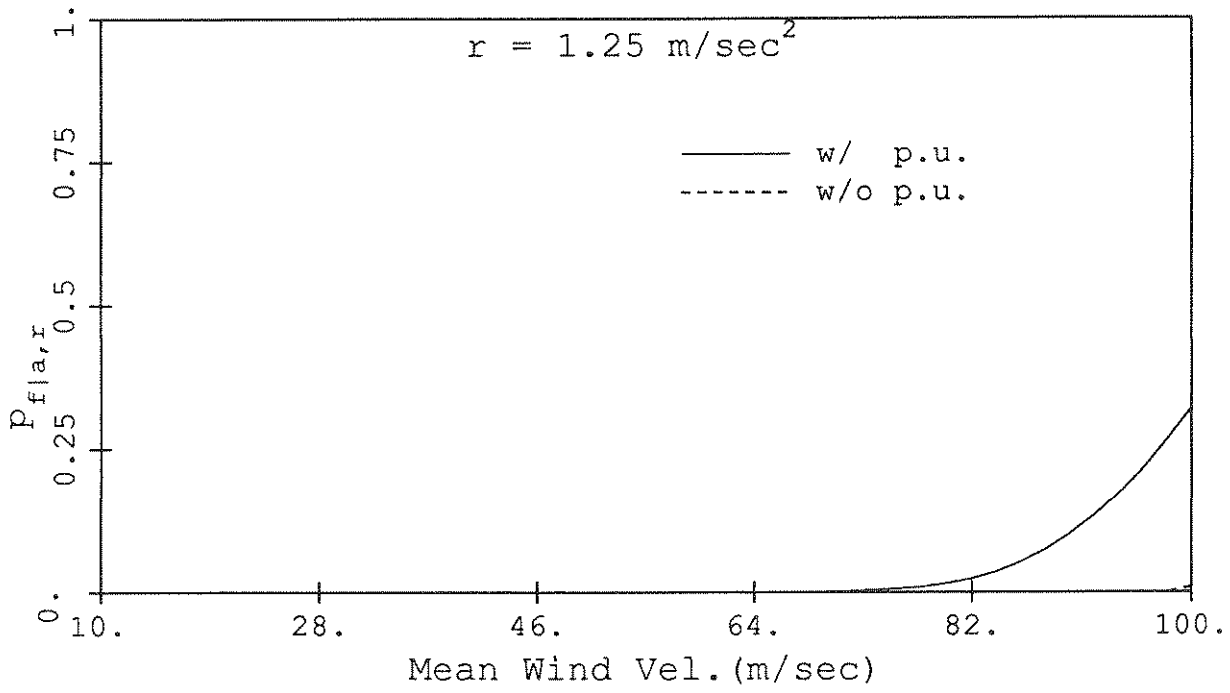

FIGURE 7-21 Conditional Failure Probability Against Sea-Storm Load Based on an Acceleration Limit State

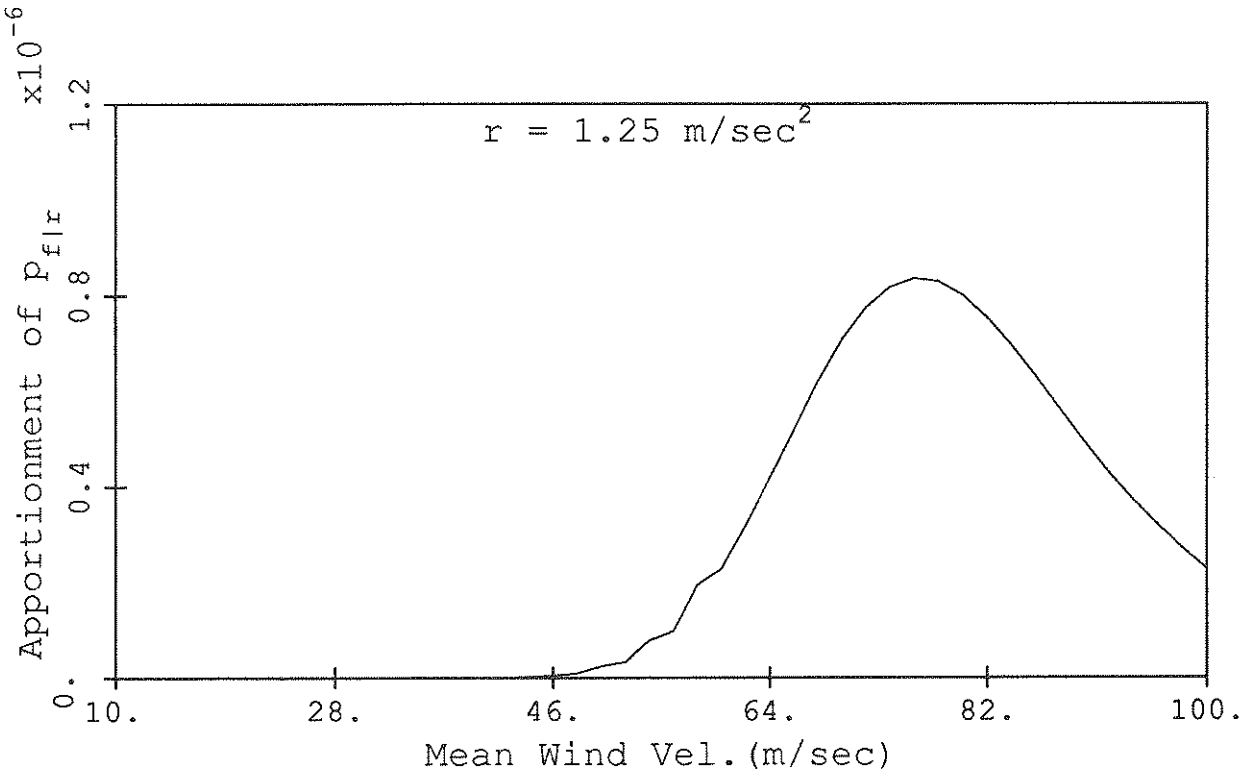

FIGURE 7-22 Conditional Failure Probability Per Event, Against Sea-Storm Load Based on an Acceleration Limit State, Apportioned Among Mean Wind Velocities

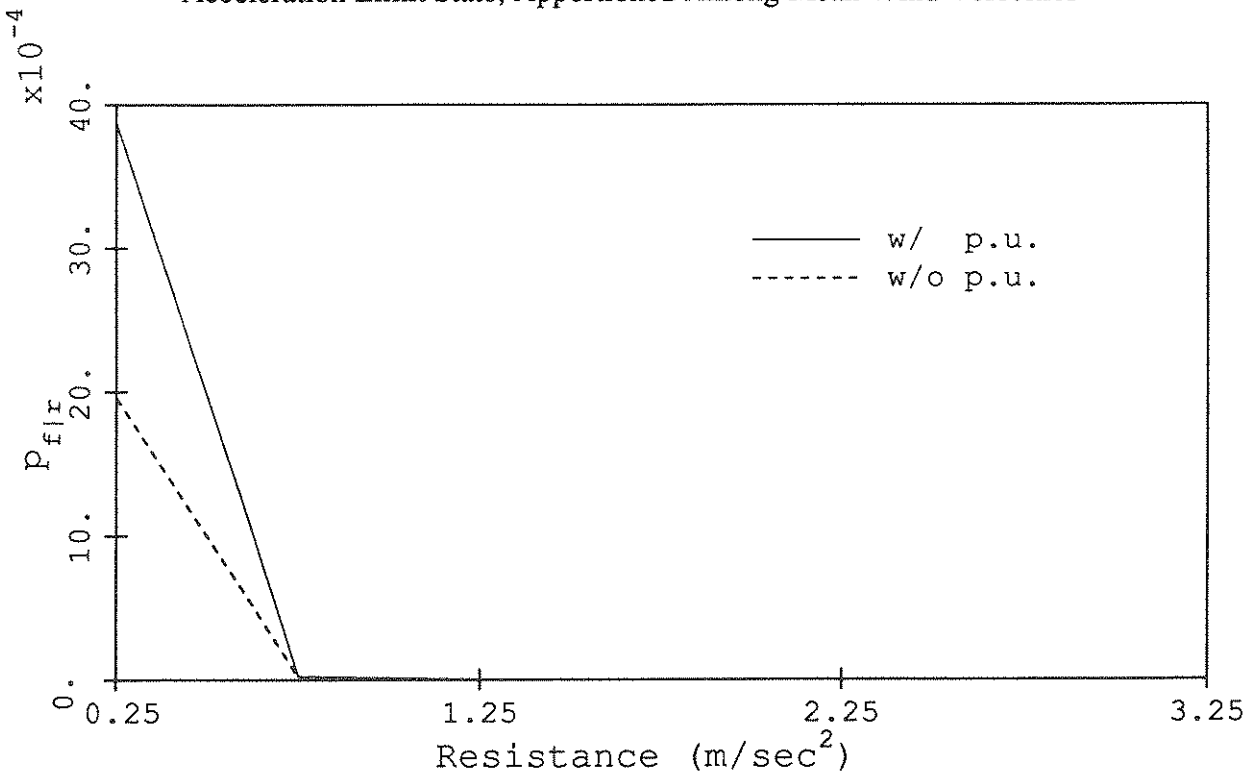

FIGURE 7-23 Conditional Failure Probability Per Event Against Sea-Storm Load Based on Displacement Limit State

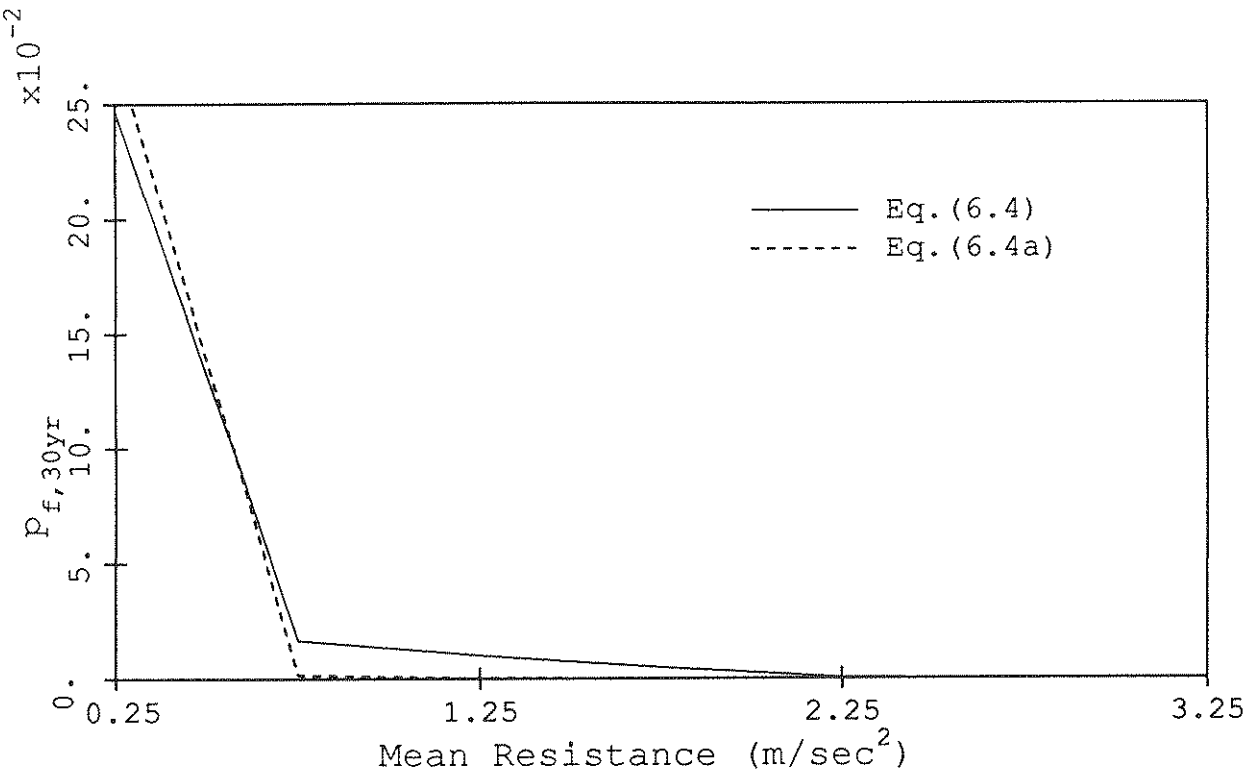

FIGURE 7-24 Overall Failure Probability in 30 Years Against Sea-Storm Load Based on Acceleration Limit State

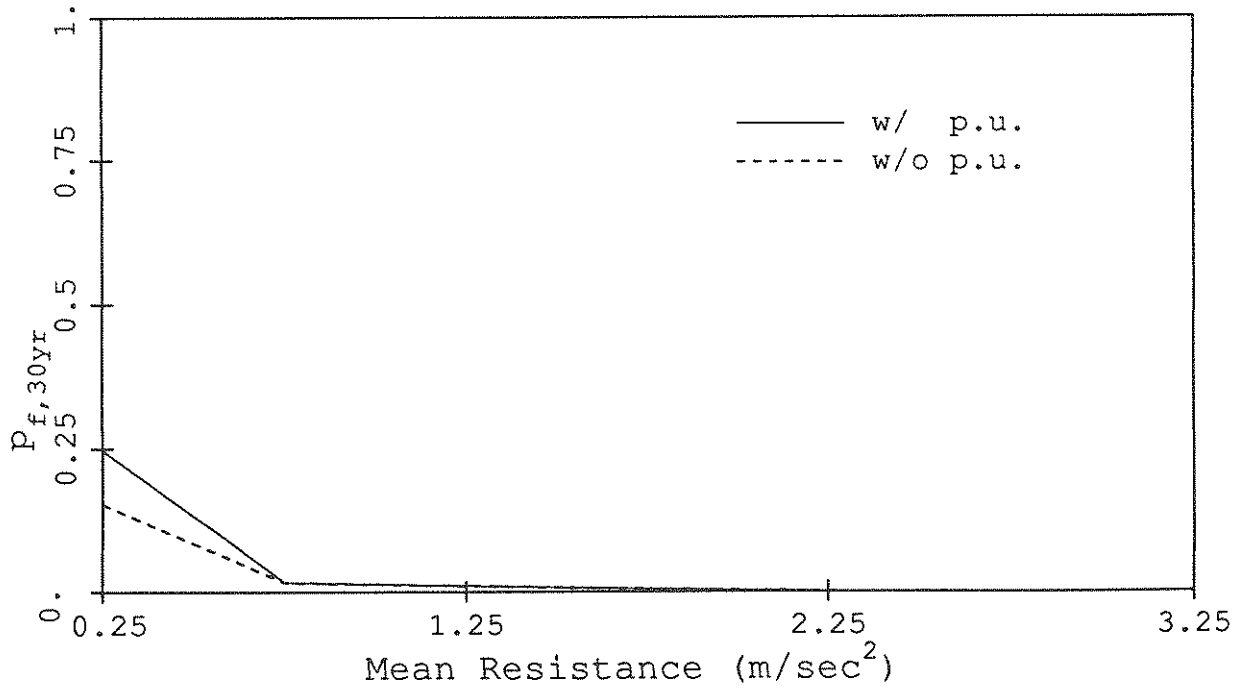

FIGURE 7-25 Overall Failure in 30 Years Against Sea-Storm Load Based on Acceleration Limit State, With and Without the Parameter Uncertainty

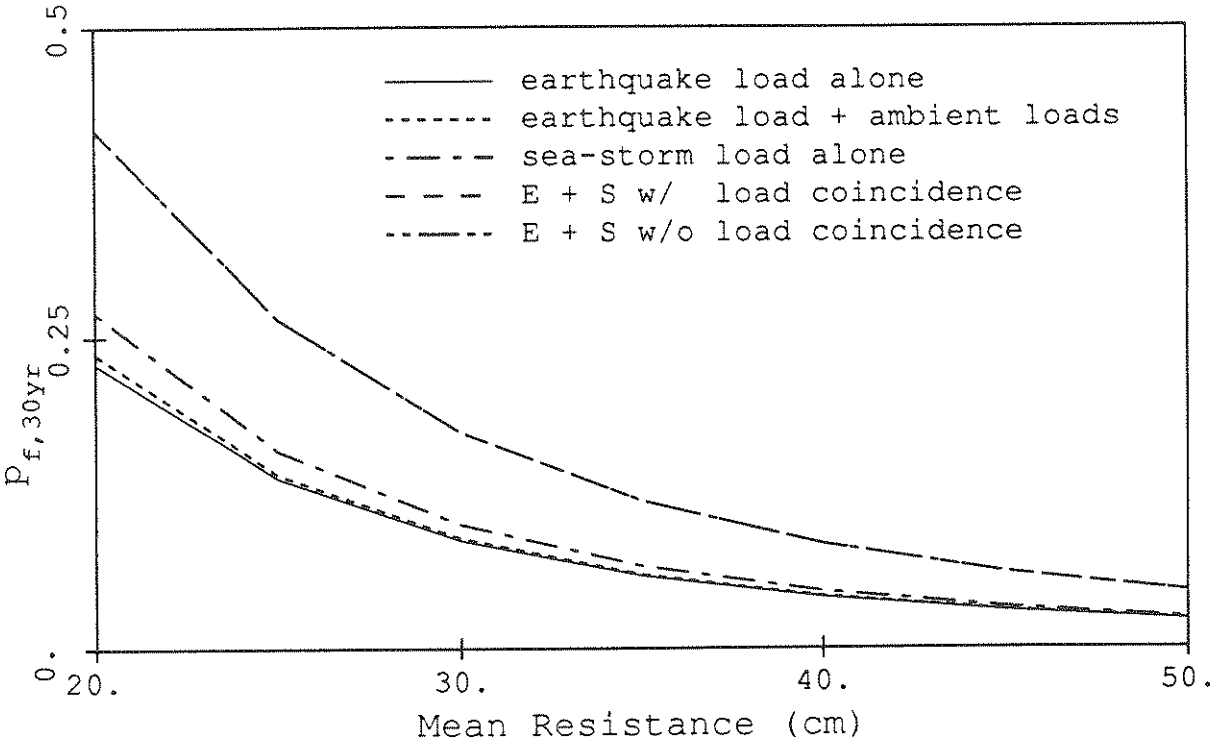

FIGURE 7-26 Overall Failure Probability in 30 Years Against Several Combinations of Loads Based on Displacement Limit State

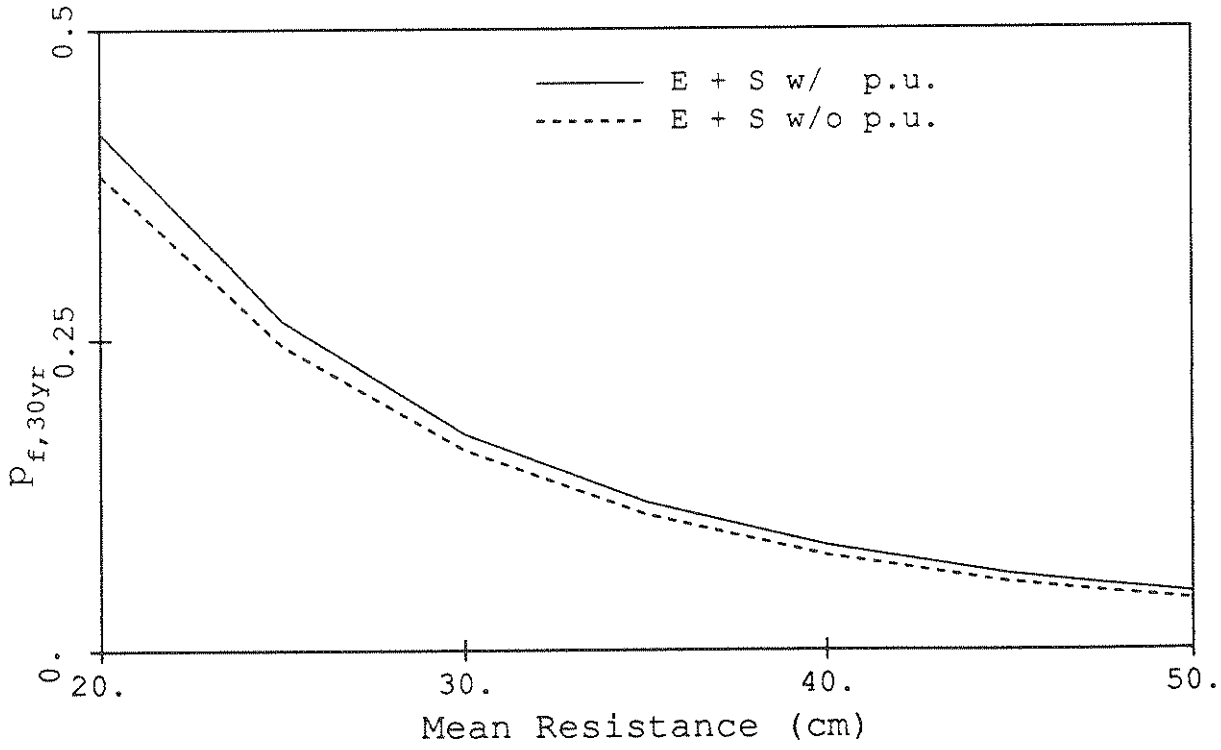

FIGURE 7-27 Overall Failure Probability in 30 Years Against Earthquake Load Plus Sea-Storm Load Based on Displacement Limit State, With and Without the Parameter Uncertainty

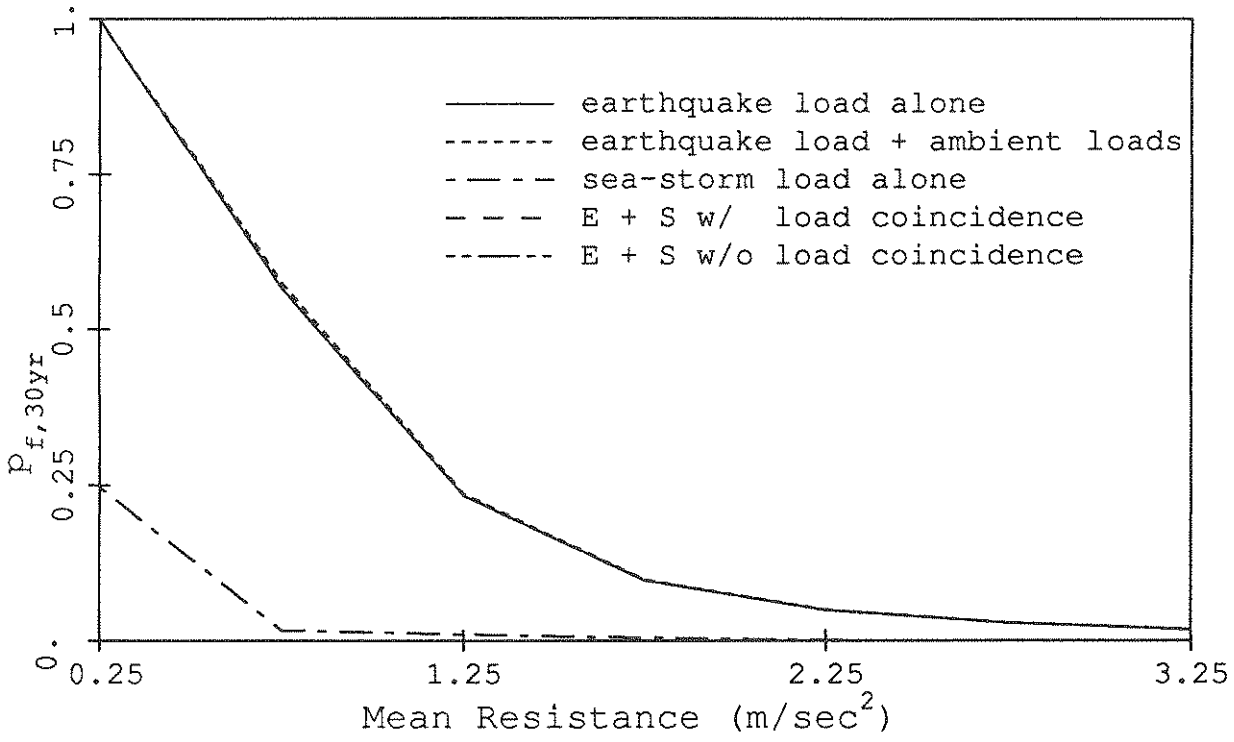

FIGURE 7-28 Overall Failure Probability in 30 Years Against Several Combinations of Loads Based on Acceleration Limit State

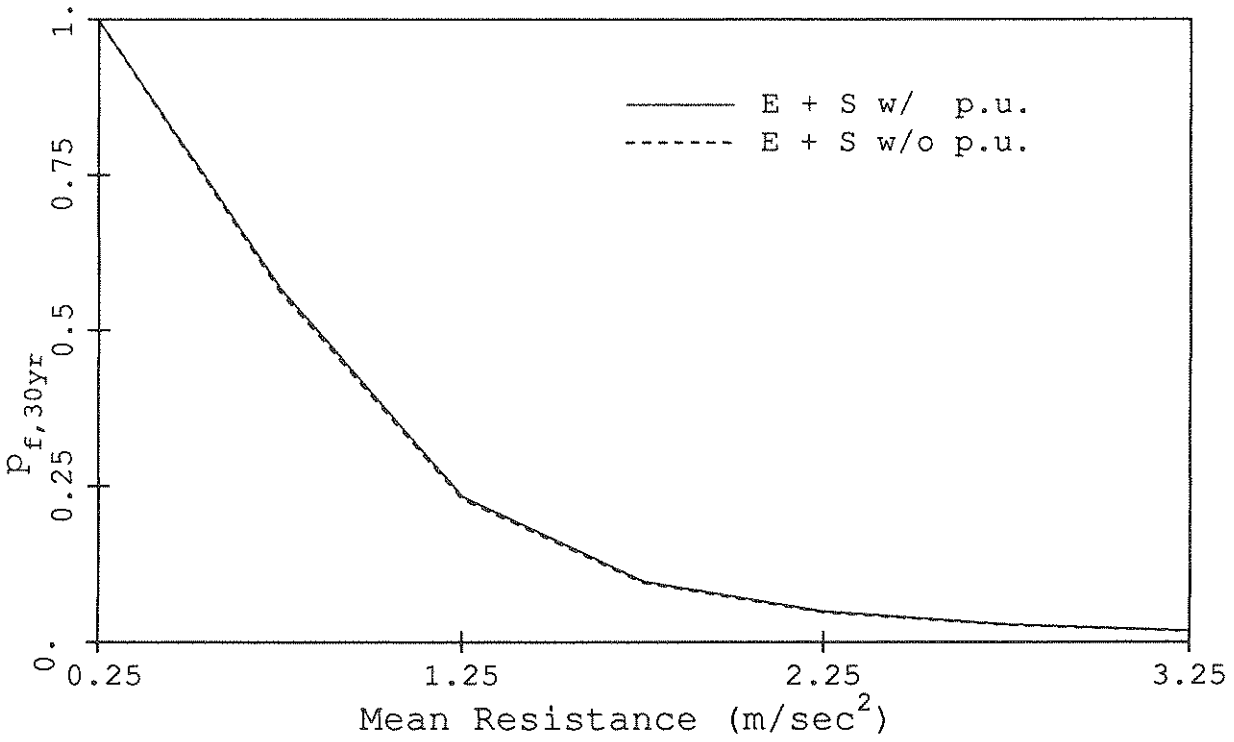

FIGURE 7-29 Overall Failure Probability in 30 Years Against Earthquake Load Plus Sea-Storm Load Based on Acceleration Limit State, With and Without the Parameter Uncertainty

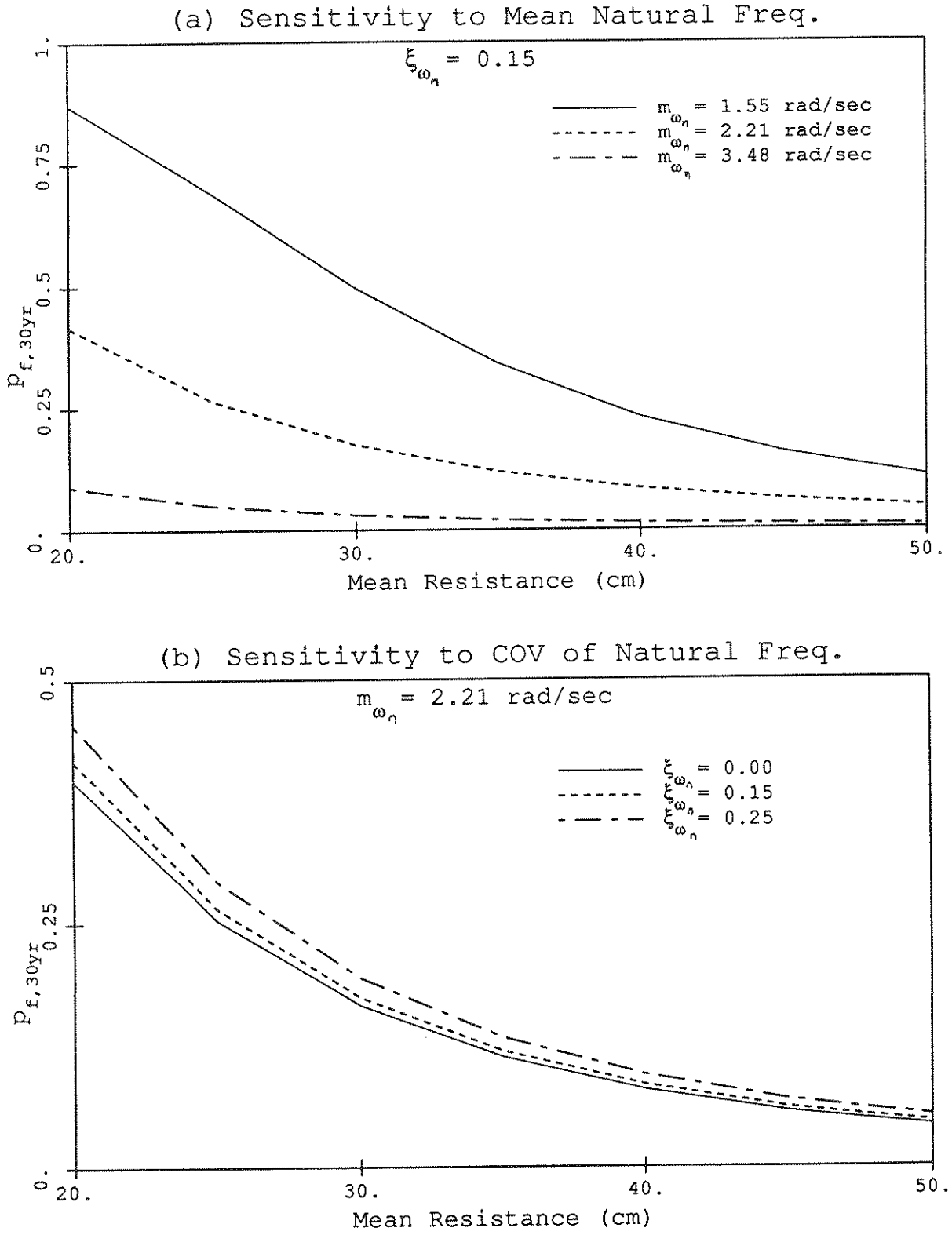

FIGURE 7-30 Sensitivity of Overall Failure Probability to the Structure's Natural Frequency Based on Displacement Limit State

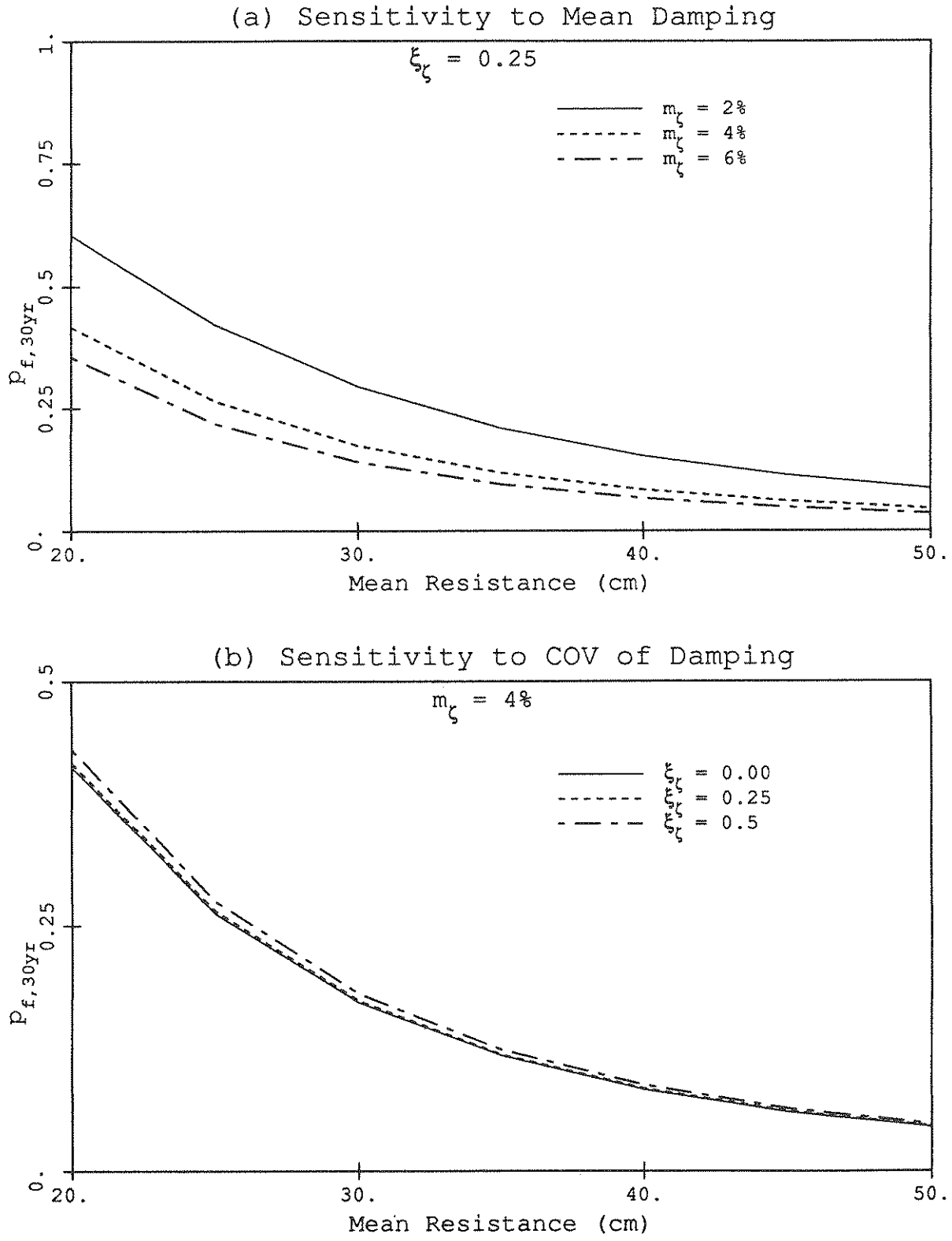

FIGURE 7-31 Sensitivity of Overall Failure Probability to the Structure's Damping Ratio Based on Displacement Limit State

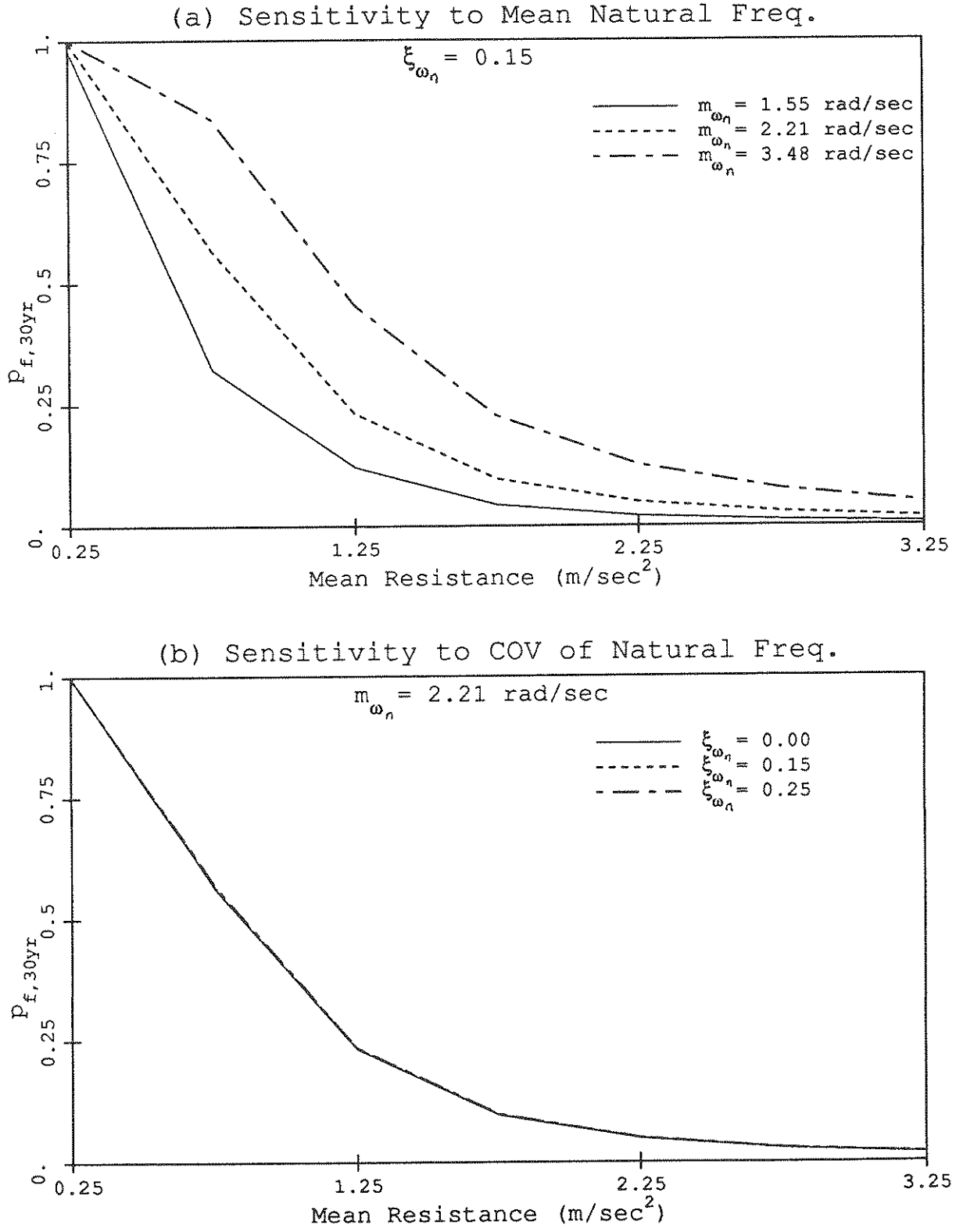

FIGURE 7-32 Sensitivity of Overall Failure Probability to the Structure's Natural Frequency Based on Acceleration Limit State

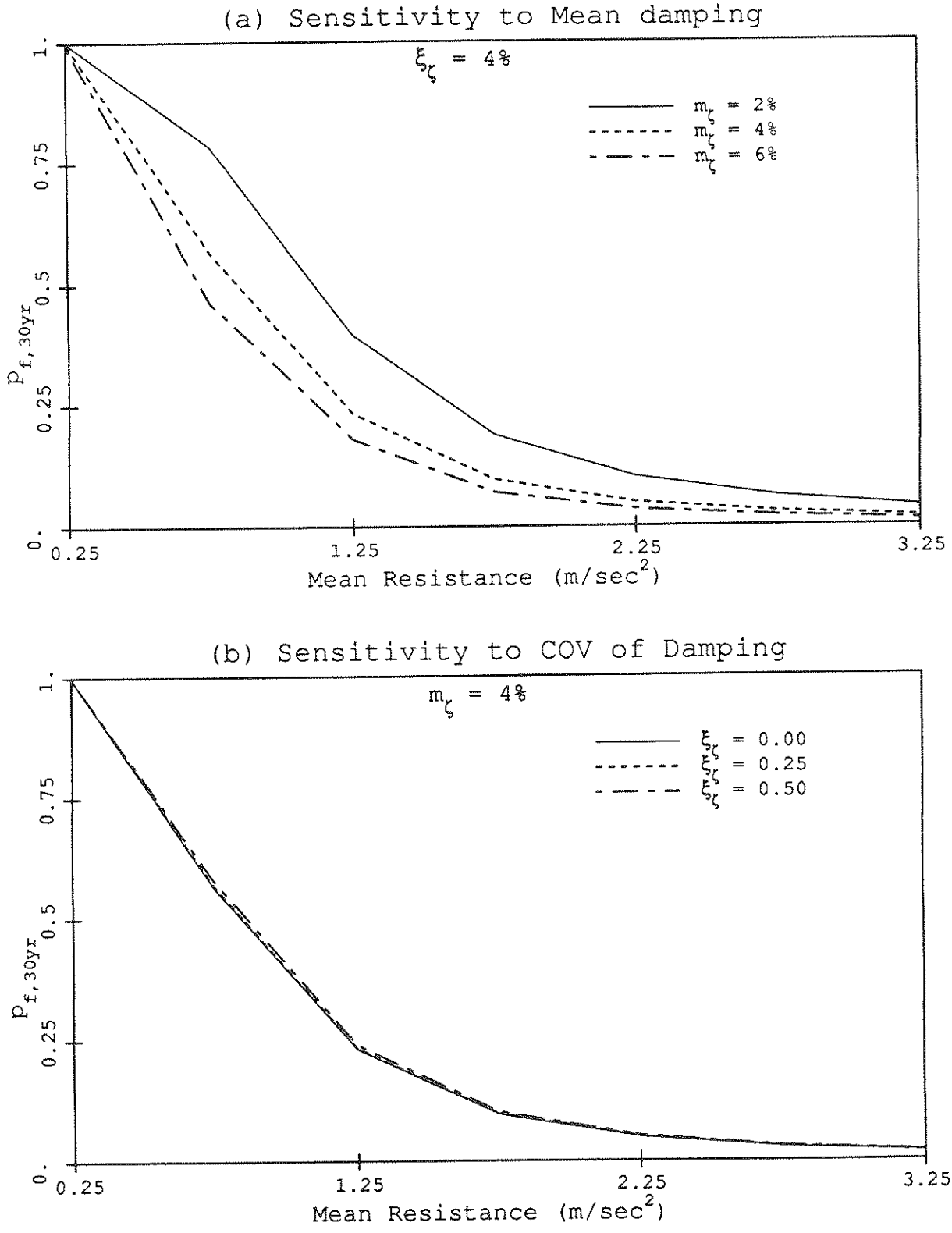

FIGURE 7-33 Sensitivity of Overall Failure Probability to the Structure's Damping Ratio Based on Acceleration Limit State

8. Conclusion

Based on two limit states, defined in terms of relative displacement and pseudo-acceleration at the deck level, and for several combinations of earthquake and sea-storm loads, this report demonstrates the short-term and long-term multi-hazard risk analysis of an offshore platform. It also determines the influence of ambient load on the earthquake safety, and the effect of parameter uncertainty on failure probabilities in general. Based on the cases studied, the following conclusions can be drawn:

1) The relative importance of loads largely depend on the limit state and the structure's natural frequency. For a flexible offshore structure, we show that while in the case of a displacement limit state the sea-storm load dominates, the same load is not important in relation to an acceleration limit state. If a deflection limit state governs the design, the margin of safety against earthquake load may be quite large.

2) The coincidental load due to the simultaneous occurrence of earthquake and sea-storm does not influence the long-term risk of offshore structures perceptibly. However, if the resistance level is very high, it could be of greater relative importance.

3) The ambient load increases the risk due to earthquake alone, especially at lower resistance levels.

4) The failure probabilities are exceedingly sensitive to the mean and the variability of a structure's natural frequency. Obtaining more and better information through ambient vibration testing or other means is likely to be very beneficial, with respect to safety and economy.

5) The statistical uncertainty of load and structural parameters affects failure probabilities in a complex manner. Depending on the load intensity, for instance, this uncertainty may either increase or decrease the conditional fragility. However, it always leads to an increase in the unconditional and overall failure probabilities. Also, the effect is sensitive to the type of limit state; in the case study, it is found to be more pronounced for the displacement limit state than for the acceleration limit state.

6) In related work in progress, we are extending the methodology to multi-degree models of the structure and to limit states that are not of the first-passage type, notably,

fatigue failure and excessive inelastic deformation. Uncertainty in event duration and the parameters of the long-term load occurrence distributions are also to be incorporated in the model.

References

1) Benjamin, J.R., and Cornell, C.A., "*Probability, Statistics, and Decision for Civil Engineers*," McGraw-Hill, New York.

2) Berge, B., and Penzien, J., "Three-dimensional stochastic response of offshore towers to wave forces," *Offshore Technology Conferences*, Dallas, Texas, OTC 2050, 1974.

3) Bernreuter, D.L., Sary, J.B., Mensing, R.W., and Chung, D.H., "Seismic hazard characterization of the Eastern United States: Methodology and interim results for ten sites," *Report for U.S. Nuclear Regulatory Commission*, NUREG/CR-3756, April 1984.

4) Davenport, A.G., "Gust loading factors," *Journal of the structural Division*, ASCE, June 1967.

5) Davenport, A.G., "Note on the random distribution of the largest value of a random function with emphasis on gust loading," *Proc. Inst. of Civil Engineers*, London, Vol. 28, 1964.

6) Kallberg, K., "Seismic risk in Southern California," *M.I.T. Dept. of Civil Engineering Research Report* R69-31, June 1969.

7) Kanai, K., "An empirical formula for the spectrum of strong earthquake motion," *Bull. Earthq. Res. Inst.*, U. of Tokyo, Vol. 39, 85–95, Tokyo.

8) Kryloff, N., and Bogoliaboff, N., "*Introduction to nonlinear mechanics: Approximate asymptotic methods*," Princeton University Press, 11, 1943.

9) Malhotra, A., and Penzien, J., "Stochastic analysis of offshore structures," *Earhquake Eng. Res. Ctr. Report No. 69-6*, U. of California, Berkeley, Calif. 1969.

10) Morison, J.R., Òbrien, M.P., Johnson, J.W., and Schaaf, S.A., "The force exerted by surface waves on piles," *Amer. Inst. Min. Eng. Petrol Trans.*, TP 2846, Vol. 189, pp. 149–154, 1950.

11) Pierson, W.J., and Moskowitz, Z., "A proposed spectral form for fully developed wind seas based on the similarity theory of S.A. Kitaigorodskii," *Journal of Geophysical Research*, Vol. 69, nr. 24, Dec. 1964.

12) Roberts, J.B., "First-passage probabilities for randomly excited systems: Diffusion methods," *Probabilistic Engineering Mechanics*, Vol. 1, N0. 2 1986.

13) Vanmarcke, E.H., "Spatial averaging of earthquake ground motion: the effect on response spectra," *Proceedings EPRI Workshop on Engineering Characterization of Small-magnitude Earthquakes*, 1987.

14) Vanmarcke, E.H., "On the distribution of the first-passage time for normal stationary random process," *Journal of Applied Mechanics*, March 1975.

15) Wen, Y.K., "Methods for reliability of structures under multiple time varying loads," *Journal of Nuclear Engineering and Design*, Vol. 60, pp. 61–70 1980.

16) Wilson, J.F., "*Dynamics of offshore structures*," John Wiley & Sons, NewYork 1984.

NATIONAL CENTER FOR EARTHQUAKE ENGINEERING RESEARCH
LIST OF PUBLISHED TECHNICAL REPORTS

The National Center for Earthquake Engineering Research (NCEER) publishes technical reports on a variety of subjects related to earthquake engineering written by authors funded through NCEER. These reports are available from both NCEER's Publications Department and the National Technical Information Service (NTIS). Requests for reports should be directed to the Publications Department, National Center for Earthquake Engineering Research, State University of New York at Buffalo, Red Jacket Quadrangle, Buffalo, New York 14261. Reports can also be requested through NTIS, 5285 Port Royal Road, Springfield, Virginia 22161. NTIS accession numbers are shown in parenthesis, if available.

NCEER-87-0001 "First-Year Program in Research, Education and Technology Transfer," 3/5/87, (PB88-134275/AS).

NCEER-87-0002 "Experimental Evaluation of Instantaneous Optimal Algorithms for Structural Control," by R.C. Lin, T.T. Soong and A.M. Reinhorn, 4/20/87, (PB88-134341/AS).

NCEER-87-0003 "Experimentation Using the Earthquake Simulation Facilities at University at Buffalo," by A.M. Reinhorn and R.L. Ketter, to be published.

NCEER-87-0004 "The System Characteristics and Performance of a Shaking Table," by J.S. Hwang, K.C. Chang and G.C. Lee, 6/1/87, (PB88-134259/AS).

NCEER-87-0005 "A Finite Element Formulation for Nonlinear Viscoplastic Material Using a Q Model," by O. Gyebi and G. Dasgupta, 11/2/87, (PB88-213764/AS).

NCEER-87-0006 "Symbolic Manipulation Program (SMP) - Algebraic Codes for Two and Three Dimensional Finite Element Formulations," by X. Lee and G. Dasgupta, 11/9/87, (PB88-219522/AS).

NCEER-87-0007 "Instantaneous Optimal Control Laws for Tall Buildings Under Seismic Excitations," by J.N. Yang, A. Akbarpour and P. Ghaemmaghami, 6/10/87, (PB88-134333/AS).

NCEER-87-0008 "IDARC: Inelastic Damage Analysis of Reinforced Concrete-Frame Shear-Wall Structures," by Y.J. Park, A.M. Reinhorn and S.K. Kunnath, 7/20/87, (PB88-134325/AS).

NCEER-87-0009 "Liquefaction Potential for New York State: A Preliminary Report on Sites in Manhattan and Buffalo," by M. Budhu, V. Vijayakumar, R.F. Giese and L. Baumgras, 8/31/87, (PB88-163704/AS).

NCEER-87-0010 "Vertical and Torsional Vibration of Foundations in Inhomogeneous Media," by A.S. Veletsos and K.W. Dotson, 6/1/87, (PB88-134291/AS).

NCEER-87-0011 "Seismic Probabilistic Risk Assessment and Seismic Margins Studies for Nuclear Power Plants," by Howard H.M. Hwang, 6/15/87, (PB88-134267/AS).

NCEER-87-0012 "Parametric Studies of Frequency Response of Secondary Systems Under Ground-Acceleration Excitations," by Y. Yong and Y.K. Lin, 6/10/87, (PB88-134309/AS).

NCEER-87-0013 "Frequency Response of Secondary Systems Under Seismic Excitation," by J.A. HoLung, J. Cai and Y.K. Lin, 7/31/87, (PB88-134317/AS).

NCEER-87-0014 "Modelling Earthquake Ground Motions in Seismically Active Regions Using Parametric Time Series Methods," G.W. Ellis and A.S. Cakmak, 8/25/87, (PB88-134283/AS).

NCEER-87-0015 "Detection and Assessment of Seismic Structural Damage," by E. DiPasquale and A.S. Cakmak, 8/25/87, (PB88-163712/AS).

NCEER-87-0016 "Pipeline Experiment at Parkfield, California," by J. Isenberg and E. Richardson, 9/15/87, (PB88-163720/AS).

NCEER-87-0017 "Digital Simulation of Seismic Ground Motion," by M. Shinozuka, G. Deodatis and T. Harada, 8/31/87, (PB88-155197/AS).

NCEER-87-0018 "Practical Considerations for Structural Control: System Uncertainty, System Time Delay and Truncation of Small Control Forces," J. Yang and A. Akbarpour, 8/10/87, (PB88-163738/AS).

NCEER-87-0019 "Modal Analysis of Nonclassically Damped Structural Systems Using Canonical Transformation," by J.N. Yang, S. Sarkani and F.X. Long, 9/27/87, (PB88-187851/AS).

NCEER-87-0020 "A Nonstationary Solution in Random Vibration Theory," by J.R. Red-Horse and P.D. Spanos, 11/3/87, (PB88-163746/AS).

NCEER-87-0021 "Horizontal Impedances for Radially Inhomogeneous Viscoelastic Soil Layers," by A.S. Veletsos and K.W. Dotson, 10/15/87, (PB88-150859/AS).

NCEER-87-0022 "Seismic Damage Assessment of Reinforced Concrete Members," by Y.S. Chung, C. Meyer and M. Shinozuka, 10/9/87, (PB88-150867/AS).

NCEER-87-0023 "Active Structural Control in Civil Engineering," by T.T. Soong, 11/11/87, (PB88-187778/AS).

NCEER-87-0024 "Vertical and Torsional Impedances for Radially Inhomogeneous Viscoelastic Soil Layers," by K.W. Dotson and A.S. Veletsos, 12/87, (PB88-187786/AS).

NCEER-87-0025 "Proceedings from the Symposium on Seismic Hazards, Ground Motions, Soil-Liquefaction and Engineering Practice in Eastern North America, October 20-22, 1987, edited by K.H. Jacob, 12/87, (PB88-188115/AS).

NCEER-87-0026 "Report on the Whittier-Narrows, California, Earthquake of October 1, 1987," by J. Pantelic and A. Reinhorn, 11/87, (PB88-187752/AS).

NCEER-87-0027 "Design of a Modular Program for Transient Nonlinear Analysis of Large 3-D Building Structures," by S. Srivastav and J.F. Abel, 12/30/87, (PB88-187950/AS).

NCEER-87-0028 "Second-Year Program in Research, Education and Technology Transfer," 3/8/88, (PB88-219480/AS).

NCEER-88-0001 "Workshop on Seismic Computer Analysis and Design of Buildings With Interactive Graphics," by J.F. Abel and C.H. Conley, 1/18/88, (PB88-187760/AS).

NCEER-88-0002 "Optimal Control of Nonlinear Flexible Structures," J.N. Yang, F.X. Long and D. Wong, 1/22/88, (PB88-213772/AS).

NCEER-88-0003 "Substructuring Techniques in the Time Domain for Primary-Secondary Structural Systems," by G. D. Manolis and G. Juhn, 2/10/88, (PB88-213780/AS).

NCEER-88-0004 "Iterative Seismic Analysis of Primary-Secondary Systems," by A. Singhal, L.D. Lutes and P. Spanos, 2/23/88, (PB88-213798/AS).

NCEER-88-0005 "Stochastic Finite Element Expansion for Random Media," P. D. Spanos and R. Ghanem, 3/14/88, (PB88-213806/AS).

NCEER-88-0006 "Combining Structural Optimization and Structural Control," F. Y. Cheng and C. P. Pantelides, 1/10/88, (PB88-213814/AS).

NCEER-88-0007 "Seismic Performance Assessment of Code-Designed Structures," H.H-M. Hwang, J-W. Jaw and H-J. Shau, 3/20/88, (PB88-219423/AS).

NCEER-88-0008 "Reliability Analysis of Code-Designed Structures Under Natural Hazards," H.H-M. Hwang, H. Ushiba and M. Shinozuka, 2/29/88.

NCEER-88-0009 "Seismic Fragility Analysis of Shear Wall Structures," J-W Jaw and H.H-M. Hwang, 4/30/88.

NCEER-88-0010 "Base Isolation of a Multi-Story Building Under a Harmonic Ground Motion - A Comparison of Performances of Various Systems," F-G Fan, G. Ahmadi and I.G. Tadjbakhsh, 5/18/88.

NCEER-88-0011 "Seismic Floor Response Spectra for a Combined System by Green's Functions," F.M. Lavelle, L.A. Bergman and P.D. Spanos, 5/1/88.

NCEER-88-0012 "A New Solution Technique for Randomly Excited Hysteretic Structures," G.Q. Cai and Y.K. Lin, 5/16/88.

NCEER-88-0013 "A Study of Radiation Damping and Soil-Structure Interaction Effects in the Centrifuge," K. Weissman, supervised by J.H. Prevost, 5/24/88.

NCEER-88-0014 "Parameter Identification and Implementation of a Kinematic Plasticity Model for Frictional Soils," J.H. Prevost and D.V. Griffiths, to be published.

NCEER-88-0015 "Two- and Three-Dimensional Dynamic Finite Element Analyses of the Long Valley Dam," D.V. Griffiths and J.H. Prevost, 6/17/88.

NCEER-88-0016 "Damage Assessment of Reinforced Concrete Structures in Eastern United States," A.M. Reinhorn, M.J. Seidel, S.K. Kunnath and Y.J. Park, 6/15/88.

NCEER-88-0017 "Dynamic Compliance of Vertically Loaded Strip Foundations in Multilayered Viscoelastic Soils," S. Ahmad and A.S.M. Israil, 6/17/88.

NCEER-88-0018 "An Experimental Study of Seismic Structural Response With Added Viscoelastic Dampers," R.C. Lin, Z. Liang, T.T. Soong and R.H. Zhang, 6/30/88.

NCEER-88-0019 "Experimental Investigation of Primary - Secondary System Interaction," G.D. Manolis, G. Juhn and A.M. Reinhorn, 5/27/88.

NCEER-88-0020 "A Response Spectrum Approach For Analysis of Nonclassically Damped Structures," J.N. Yang, S. Sarkani and F.X. Long, 4/22/88.

NCEER-88-0021 "Seismic Interaction of Structures and Soils: Stochastic Approach," A.S. Veletsos and A.M. Prasad, 7/21/88.

NCEER-88-0022 "Identification of the Serviceability Limit State and Detection of Seismic Structural Damage," E. DiPasquale and A.S. Cakmak, 6/15/88.

NCEER-88-0023 "Multi-Hazard Risk Analysis: Case of a Simple Offshore Structure," B.K. Bhartia and E.H. Vanmarcke, 7/21/88.